

CONCEPT-BASED ADVERSARIAL ATTACK: A PROBABILISTIC PERSPECTIVE

Andi Zhang*
University of Warwick
University of Manchester
az381@cantab.ac.uk

Xuan Ding
The Chinese University of Hong Kong, Shenzhen
202322011119@mail.bnu.edu.cn

Steven McDonagh
University of Edinburgh
s.mcdonagh@ed.ac.uk

Samuel Kaski
University of Manchester
University of Aalto
samuel.kaski@aalto.fi

ABSTRACT

We propose a concept-based adversarial attack framework that extends beyond single-image perturbations by adopting a probabilistic perspective. Rather than modifying a single image, our method operates on an entire concept — represented by a distribution — to generate diverse adversarial examples. Preserving the concept is essential, as it ensures that the resulting adversarial images remain identifiable as instances of the original underlying category or identity. By sampling from this concept-based adversarial distribution, we generate images that maintain the original concept but vary in pose, viewpoint, or background, thereby misleading the classifier. Mathematically, this framework remains consistent with traditional adversarial attacks in a principled manner. Our theoretical and empirical results demonstrate that concept-based adversarial attacks yield more diverse adversarial examples and effectively preserve the underlying concept, while achieving higher attack efficiency. Code and examples can be found at <https://github.com/andiac/ConceptAdv>.

1 INTRODUCTION

Adversarial attacks aim to deceive a classifier while preserving the original meaning of the input object (Dalvi et al., 2004; Lowd & Meek, 2005a;b; Biggio & Roli, 2018). We refer to the manipulated instance as an adversarial example. Early work by Szegedy et al. (2014) and Goodfellow et al. (2015) introduced adversarial attacks against deep learning models for images.

In the image-based adversarial setting, it is widely accepted that controlling the geometric distance between the adversarial example and its original image is crucial for maintaining the original image’s meaning. Consequently, many adversarial attack algorithms constrain perturbations using norms such as L_1 , L_2 , or L_∞ . Moreover, given the rapid progress in machine learning research, fair comparisons across different adversarial methods have become essential. Numerous benchmarks and competitions (Madry et al., 2018; Croce et al., 2020; Dong et al., 2021) therefore focus on attack success rates under the constraint that geometric distance does not exceed a threshold δ .

However, as adversarial defense techniques improve, small geometric perturbations alone increasingly fail to generate adversarial examples that reliably fool classifiers, particularly when strong transferability is required (Song et al., 2018; Xiao et al., 2018b; Bhattad et al., 2020). This shortcoming has led researchers to explore unrestricted adversarial attacks, which involve larger geometric perturbations. Although “unrestricted” implies that adversarial examples need not be bounded by strict geometric distance, these examples must still remain faithful to the semantics of the original image; otherwise, the core goal of preserving the input’s meaning is lost.

*Corresponding Author.

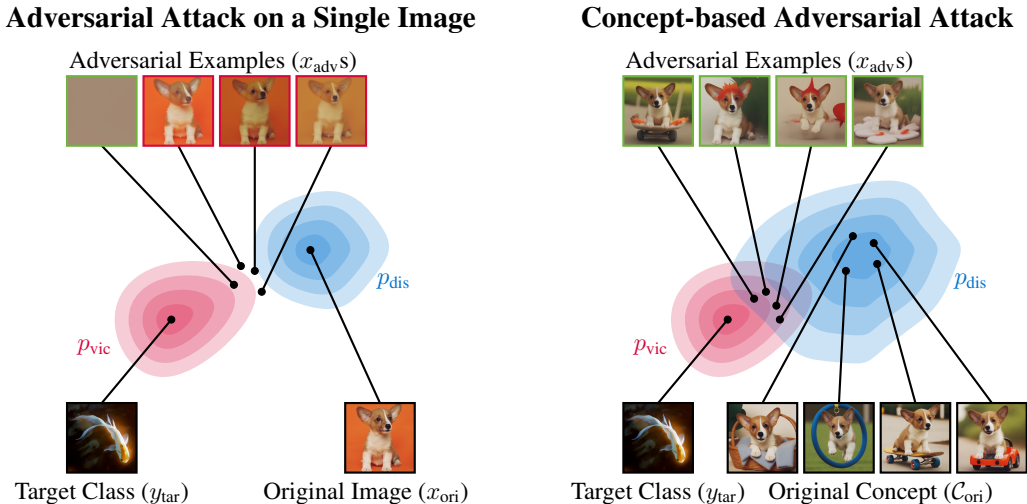


Figure 1: Comparison of a single-image adversarial attack (left) versus our proposed concept-based adversarial attack (right). In both cases, adversarial examples x_{adv} are drawn from the product of a distance distribution p_{dis} and a victim distribution p_{vic} . On the left, p_{dis} is centered on a single image x_{ori} , so its overlap with p_{vic} is small. Consequently, adversarial examples that successfully fool the victim classifier typically lose the original image’s meaning, whereas those that preserve the original meaning fail to deceive the classifier. In contrast, on the right, p_{dis} spans the original concept C_{ori} , greatly increasing overlap with p_{vic} . As a result, the generated adversarial examples both maintain the concept’s meaning and easily deceive the classifier. (A green image border indicates an example that successfully fools the classifier; red indicates failure.)

Zhang et al. (2024b) introduced a probabilistic perspective on adversarial attacks, demonstrating that traditional geometric constraints can be interpreted as specific “distance” distributions p_{dis} . Under this view, generating adversarial examples amounts to sampling from the product of p_{dis} and the “victim” distribution p_{vic} , which represents the target classifier under attack. Importantly, p_{dis} need not be induced solely by geometric distance. Instead, one can fit a probabilistic generative model (PGM) around the original image, allowing the PGM’s semantic representation to implicitly define a semantics-based notion of distance. As illustrated on the left side of Figure 1, Zhang et al. (2024b) indicate that p_{dis} should be centered on the original image.

Building on Zhang et al. (2024b)’s probabilistic perspective, we expand the distance distribution p_{dis} from operating on a single image to operating on an entire concept, which can be represented by a probability distribution over images that correspond to the same underlying object, identity or category. As shown on the right side of Figure 1, this generalization introduces a new class of adversarial attacks. Rather than perturbing a single image, we generate a fresh image that captures the same underlying concept yet deceives the classifier. We refer to this approach as a concept-based adversarial attack. Mathematically, it remains consistent with traditional adversarial attacks when viewed under the probabilistic framework. As we demonstrate, broadening the distance distribution to concept-level information reduces its gap from the victim distribution p_{vic} , resulting in substantially higher attack success rates.

Our main contributions are as follows:

- **Concept-based adversarial attack:** We introduce a new type of adversarial attack that moves beyond single-image perturbations to a concept represented by a distribution, this new approach aligns with traditional adversarial attacks in a principled manner.
- **Concept augmentation:** We propose a practical concept augmentation strategy using modern generative models, enhancing the diversity of the distance distribution.
- **Theoretical and empirical validation:** We provide both theoretical proof and experimental evidence showing that expanding the attack from a single image to an entire concept reduces the distance between p_{vic} and p_{dis} , boosting the attack efficiency.

- **Higher success rates:** Our experiments confirm that concept-based adversarial attacks achieve higher targeted attack success rates while preserving the original concept.
- **Practical Guidelines and Scenarios:** We provide practical guidelines and example application scenarios, detailed in Appendix K.

2 PRELIMINARIES

2.1 PROBABILISTIC GENERATIVE MODELS (PGMS) AND THEIR LIKELIHOODS

The goal of probabilistic generative models is to learn a parameterized distribution p_θ that approximates the true distribution p . In practice, we only observe a finite dataset $\mathcal{D} = \{x_1, \dots, x_n\}$, and training is typically done by maximizing its likelihood. For image modeling, popular approaches such as VAEs (Kingma et al., 2013) and diffusion models (Song & Ermon, 2019; Ho et al., 2020) optimize a lower bound on the log-likelihood (the ELBO) rather than the likelihood itself. Thus, likelihood estimation in practice amounts to computing this ELBO (Burda et al., 2015; Nalisnick et al., 2019).

2.2 ADVERSARIAL ATTACK

Given a classifier $C : [0, 1]^n \rightarrow \mathcal{Y}$, where n is the input dimension and \mathcal{Y} is the label space, consider an original image $x_{\text{ori}} \in [0, 1]^n$ and a target label $y_{\text{tar}} \in \mathcal{Y}$. The goal of a targeted adversarial attack is to construct an adversarial example x_{adv} such that $C(x_{\text{adv}}) = y_{\text{tar}}$ while keeping x_{adv} close to x_{ori} . The corresponding optimization problem is

$$\min \mathcal{D}(x_{\text{ori}}, x_{\text{adv}}) \quad \text{subject to} \quad C(x_{\text{adv}}) = y_{\text{tar}} \quad \text{and} \quad x_{\text{adv}} \in [0, 1]^n,$$

where \mathcal{D} measures the distance (similarity) between x_{ori} and x_{adv} , typically via an \mathcal{L}_1 , \mathcal{L}_2 , or \mathcal{L}_∞ norm. Directly solving this constrained optimization can be challenging. To address this, Szegedy et al. (2014) propose a relaxation:

$$\min \mathcal{D}(x_{\text{ori}}, x_{\text{adv}}) + c f(x_{\text{adv}}, y_{\text{tar}}) \quad \text{subject to} \quad x_{\text{adv}} \in [0, 1]^n, \quad (1)$$

where c is a constant, and f is an objective function that guides the classifier’s predictions toward the target label. In Szegedy et al. (2014)’s work, f is taken to be the cross-entropy loss; Carlini & Wagner (2017) present additional choices for f .

2.3 PROBABILISTIC ADVERSARIAL ATTACK

By employing Langevin Dynamics as an optimizer for equation 1, Zhang et al. (2024b) derive a probabilistic perspective on adversarial attacks. They introduce the adversarial distribution:

$$p_{\text{adv}}(x_{\text{adv}} \mid x_{\text{ori}}, y_{\text{tar}}) \propto p_{\text{vic}}(x_{\text{adv}} \mid y_{\text{tar}}) p_{\text{dis}}(x_{\text{adv}} \mid x_{\text{ori}}), \quad (2)$$

where $p_{\text{vic}}(x_{\text{adv}} \mid y_{\text{tar}}) \propto \exp(-c f(x_{\text{adv}}, y_{\text{tar}}))$ is the “victim” distribution emphasizing misclassification toward y_{tar} , and $p_{\text{dis}}(x_{\text{adv}} \mid x_{\text{ori}}) \propto \exp(-\mathcal{D}(x_{\text{ori}}, x_{\text{adv}}))$ is the “distance” distribution around x_{ori} . This formulation leverages the fact that Langevin Dynamics converges to the corresponding Gibbs distribution (Lamperski, 2021), thereby providing a probabilistic interpretation of adversarial attack generation.

This probabilistic perspective aligns with traditional geometry-based adversarial attacks. For example, if \mathcal{D} is the \mathcal{L}_1 norm, then $p_{\text{dis}}(x_{\text{adv}} \mid x_{\text{ori}}) \propto \exp(-\|x_{\text{adv}} - x_{\text{ori}}\|_1)$ takes the form of a Laplace distribution. Similarly, if \mathcal{D} is the squared \mathcal{L}_2 norm, then $p_{\text{dis}}(x_{\text{adv}} \mid x_{\text{ori}}) \propto \exp(-\|x_{\text{adv}} - x_{\text{ori}}\|_2^2)$ is a Gaussian distribution.

Zhang et al. (2024b) indicate that the distance distribution p_{dis} can be any distribution centered around x_{ori} , meaning the choice of p_{dis} implicitly defines the distance \mathcal{D} . Consequently, using a PGM centered on x_{ori} as p_{dis} yields a semantic-aware notion of distance. By then sampling from the corresponding adversarial distribution p_{adv} , one can generate semantic-aware adversarial examples.

3 CONCEPT-BASED ADVERSARIAL ATTACK

3.1 CONCEPT DISTRIBUTION

We aim to extend adversarial attacks from operating on a single original image to operating on an original concept \mathcal{C}_{ori} . A concept is inherently abstract and subjective: it may refer to a specific physical object (e.g., a rubber duck), a particular identity such as the long-eared corgi puppy with a lighter left cheek shown in Figure 1, or a broader class such as “corgi,” regardless of age, size, or specific attributes. **Although defining a concept in an absolute sense is difficult (Poeta et al., 2023), we can represent it through a concept distribution**, denoted by $p(\cdot | \mathcal{C}_{\text{ori}})$.

This distribution serves as an interface through which users can specify what the concept is. In practice, we recommend two ways for users to instantiate their notion of a concept:

- **Direct specification of a concept distribution:** The user may already possess a generative model or any other mechanism that directly provides a distribution $p(\cdot | \mathcal{C}_{\text{ori}})$ representing the concept.
- **Constructing the distribution from an image set:** The user may collect a set of images depicting the desired concept (e.g., different poses of the same corgi in Figure 1), and then train or fine-tune a probabilistic generative model (PGM) on this set to obtain the corresponding concept distribution $p(\cdot | \mathcal{C}_{\text{ori}})$. Here, \mathcal{C}_{ori} is a set of images $\mathcal{C}_{\text{ori}} = \{x_{\text{ori}}^{(1)}, \dots, x_{\text{ori}}^{(K)}\}$, where K is the number of images depicting \mathcal{C}_{ori} .

In the remainder of this paper, we demonstrate the second approach, as it allows us to clearly showcase how concept-level information can be incorporated into adversarial attacks using accessible image data and standard generative modeling pipelines.

3.2 CONCEPT DISTRIBUTION AS A DISTANCE DISTRIBUTION

Building on the probabilistic perspective of adversarial attacks (Zhang et al., 2024b), a distribution used as a distance distribution can implicitly define a notion of distance. Therefore, by using the concept distribution defined in the previous subsection as the distance distribution, we implicitly define the distance between an adversarial example and the underlying concept. Formally,

$$p_{\text{adv}}(x_{\text{adv}} | \mathcal{C}_{\text{ori}}, y_{\text{tar}}) \propto p_{\text{vic}}(x_{\text{adv}} | y_{\text{tar}}) p_{\text{dis}}(x_{\text{adv}} | \mathcal{C}_{\text{ori}}) \quad (3)$$

where $p_{\text{adv}}(\cdot | \mathcal{C}_{\text{ori}}, y_{\text{tar}})$ is the adversarial distribution relative to the concept \mathcal{C}_{ori} and the target label y_{tar} . The distance distribution $p_{\text{dis}}(\cdot | \mathcal{C}_{\text{ori}})$ is the concept distribution.

Comparing (2) and (3) shows that the only modification is replacing x_{ori} with \mathcal{C}_{ori} . Hence, the probabilistic adversarial attack (Zhang et al., 2024b) is the special case $\mathcal{C}_{\text{ori}} = \{x_{\text{ori}}\}$ (i.e., $|\mathcal{C}_{\text{ori}}| = 1$). This straightforward and compact expansion allows us to heavily reuse the implementation of the probabilistic adversarial attack, making probabilistic adversarial attack (ProbAttack¹) a natural ablation baseline for our method.

While intuition suggests that expanding the perturbation space should produce stronger adversarial examples, rigorous justification is needed. In the following sections, we adopt the probabilistic perspective, presenting both theoretical analysis and empirical evidence to demonstrate how this expansion enhances attack effectiveness without compromising perceptual quality.

3.3 CONCEPT-BASED ADVERSARIAL ATTACKS GENERATE HIGHER QUALITY ADVERSARIAL EXAMPLES

From the probabilistic perspective, generating adversarial examples amounts to sampling from the overlap between p_{vic} and p_{dis} , since p_{adv} is proportional to their product (Hinton, 2002). For the common case of attacking a single original image x_{ori} , this procedure is illustrated on the left side of Figure 1. Empirical research has shown that modern robust classifiers can produce high-quality

¹Both Zhang et al. (2024b) and our work present a methodology applicable to any PGM (e.g., VAE, energy-based, or diffusion). Since diffusion models are the most powerful PGMs, we adopt them throughout this paper. We use ProbAttack to denote the diffusion-based implementation of Zhang et al. (2024b).

images of the target classes (Santurkar et al., 2019; Zhang et al., 2024b; Zhu et al., 2021), causing p_{vic} to concentrate on the semantics of those classes. Consequently, as x_{ori} does not depict the target class, the intersection between p_{vic} and p_{dis} is small. Since high-quality images rarely appear in low-density regions of the distribution, the resulting adversarial examples drawn from this limited intersection tend to be of lower quality.

We claim that our concept-based adversarial attacks reduce the distance between the p_{vic} and the p_{dis} , thereby increasing their overlap. This broader overlap yields higher-quality adversarial examples and improves targeted attack success rates, as illustrated on the right side of Figure 1.

To justify this claim, we must address two key questions:

- Do concept-based adversarial attacks indeed decrease the distance between p_{vic} and p_{dis} ?
- Do they genuinely produce better adversarial examples?

The remainder of this paper focuses on answering these questions.

3.4 THE DISTANCE BETWEEN DISTRIBUTIONS: A THEORETICAL STUDY

In the whitebox adversarial attack scenario, both the victim classifier and target label are provided, which means p_{vic} remains fixed. Let $p_{\text{dis}}(\cdot | \mathcal{C}_{\text{ori}})$ be a Gibbs distribution of the form $p_{\text{dis}}(x | \mathcal{C}_{\text{ori}}) \propto \exp(-\beta D(x, \mu))$, where D is a distance function measuring the discrepancy between a point x and the concept center μ . The following theorem shows that, under suitable conditions, increasing the dispersion of p_{dis} (i.e., decreasing β^2) reduces the KL divergence between p_{vic} and p_{dis} :

Theorem 1. *Let p be a probability distribution and q be a Gibbs distribution of the form*

$$q(x) = \frac{\exp(-\beta D(x, \mu))}{Z(\beta)},$$

where $Z(\beta)$ is the normalizing constant, μ is a constant and D is a distance function. Then $KL(p || q)$ is a increasing function of β whenever $\mathbb{E}_{X \sim p}[D(X, \mu)] > \mathbb{E}_{X \sim q}[D(X, \mu)]$.

The proof is provided in Appendix A. By Theorem 1, we see that $KL(p_{\text{vic}} || p_{\text{dis}})$ decreases as β decreases, provided that $\mathbb{E}_{X \sim p}[D(X, \mu)] > \mathbb{E}_{X \sim q}[D(X, \mu)]$. In the probabilistic adversarial attack framework, this condition is always satisfied because samples drawn from p_{vic} lie farther from the mean of p_{dis} than samples drawn from p_{dis} itself. If this were not the case, the fundamental assumption that p_{dis} represents a distance distribution concentrated around x_{ori} or \mathcal{C}_{ori} would be violated.

In practice, different PGMs may be used to model p_{dis} . When an energy-based model (EBM) is adopted, it explicitly learns a Gibbs distribution (LeCun et al., 2006). When a diffusion model (via score matching) is used, it instead learns an implicit representation of the corresponding energy function (Song & Ermon, 2019). Consequently, treating p_{dis} as a Gibbs distribution in this section is fully consistent with practical implementations, and is also aligned with the probabilistic adversarial attack formulation in Section 2.3.

3.5 THE DISTANCE BETWEEN DISTRIBUTIONS: AN EMPIRICAL STUDY

The following theorem provides a tractable expression for the difference in KL divergence between a fixed victim distribution and two different distance distributions.

Theorem 2. *Let $p_{\text{dis}}^{(1)} = p_{\text{dis}}(\cdot | \mathcal{C}_{\text{ori}}^{(1)})$ and $p_{\text{dis}}^{(2)} = p_{\text{dis}}(\cdot | \mathcal{C}_{\text{ori}}^{(2)})$ be two distance distributions, and let $p_{\text{vic}}(\cdot | y_{\text{tar}})$ be the victim distribution corresponding to a victim classifier $p(y_{\text{tar}} | x)$. Then, the difference*

$$\Delta := KL(p_{\text{dis}}^{(1)} || p_{\text{vic}}) - KL(p_{\text{dis}}^{(2)} || p_{\text{vic}})$$

is given by

$$\Delta = \mathbb{E}_{X \sim p_{\text{dis}}^{(1)}} [\log p_{\text{dis}}^{(1)}(X) - c \log p(y_{\text{tar}} | X)] - \mathbb{E}_{X \sim p_{\text{dis}}^{(2)}} [\log p_{\text{dis}}^{(2)}(X) - c \log p(y_{\text{tar}} | X)].$$

²A smaller β corresponds to a higher ‘‘temperature’’ in the Gibbs distribution, which makes p_{dis} more dispersed.

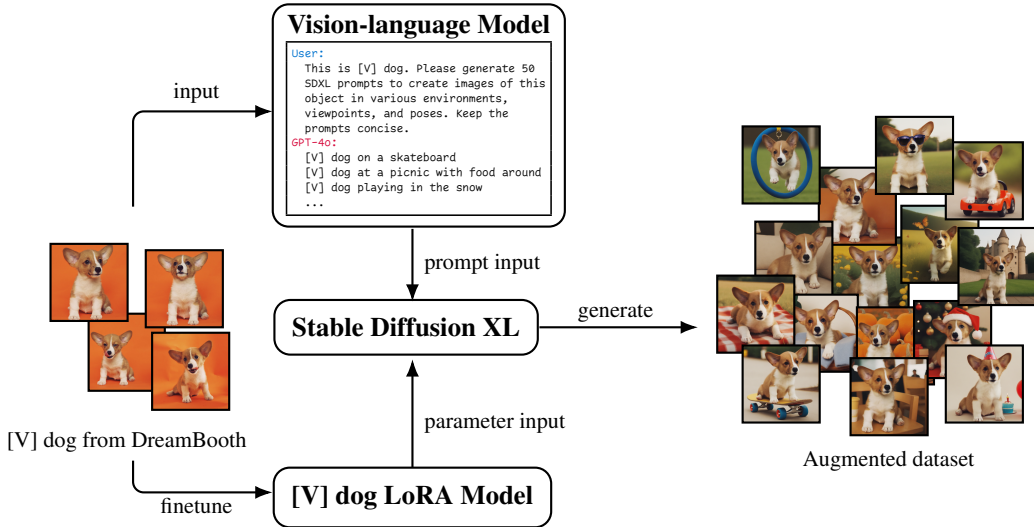


Figure 2: Illustration of how a single corgi concept (“[V] dog”) is expanded into a diverse dataset. DreamBooth images (left) are finetuned with LoRA in Stable Diffusion XL, guided by GPT-4o prompts, to generate various poses, viewpoints, and environments (right).

The proof is provided in Appendix A. We estimate Δ via Monte Carlo integration and further reduce variance by using common random numbers in the sampling process; details of such practical techniques are introduced in Appendix B. In section 5.3, we empirically show that, concept-based adversarial attacks reduce the distance between distributions p_{vic} and p_{dis} by showing $\Delta < 0$ when $p_{dis}^{(2)}$ is a distance distribution around only one image and $p_{dis}^{(1)}$ is a distance distribution around a concept.

4 GENERATING CONCEPT-BASED ADVERSARIAL EXAMPLES

In this section we introduce some practical methods to generate concept-based adversarial examples.

4.1 AUGMENT CONCEPT DATASETS BY MODERN GENERATIVE MODELS

In practice, it can be somewhat challenging to obtain a high-quality, highly diverse dataset \mathcal{C}_{ori} depicting the same concept, as required by our method. For example, as shown on the left side of Figure 2, the dataset provided by DreamBooth (Ruiz et al., 2023) contains four images of the same long-eared corgi. Although the corgi is shown in various poses and from multiple viewpoints, the relatively uniform backgrounds do not provide sufficient diversity for our concept-based adversarial attack. Therefore, we decided to use Stable Diffusion XL (Podell et al., 2023) to expand the concept-description dataset.

As illustrated in Figure 2, we designate the corgi as “[V] dog”. Using LoRA finetuning (Hu et al., 2022), we train an SDXL LoRA model on this concept. Next, we feed the five corgi images into GPT-4o (Hurst et al., 2024), stating that these images represent the “[V] dog” and asking it to produce SDXL prompts that embody sufficient diversity for the “[V] dog.” Finally, we load the corgi LoRA into SDXL and, guided by GPT-4o’s prompts (on the top of Figure 2), generate images featuring a wide range of viewpoints, environments, and poses for this corgi concept (see the right side of Figure 2).

4.2 SAMPLE SELECTION

A key advantage of probabilistic adversarial attacks is that we can draw multiple samples from p_{adv} and select the best ones³. In a white-box scenario, we can simply discard samples that fail to deceive the classifier (rejection sampling). However, if p_{dis} and p_{vic} overlap only slightly, this may lead to high rejection rates (especially under a top-1 success criterion).

As a workaround, we first sample M adversarial examples from p_{adv} and select the best among them. For small batches, it is feasible to manually choose which examples preserve the original concept. However, because we need a large number of adversarial examples, we use an automated approach: we sort the samples by how highly they rank the target class and, in the event of a tie, we employ one of two strategies — referred to here as the “conservative strategy” (CONS) and the “aggressive strategy” (AGGR). Under the conservative strategy, we pick the example with the lowest softmax probability, thereby filtering out samples that deviate significantly from the original concept. Under the aggressive strategy, we pick the example with the highest softmax probability, helping us select samples with the greatest adversarial potential.

5 EXPERIMENTS

5.1 DATA PREPARATION

We use the DreamBooth dataset (Ruiz et al., 2023), which provides 30 objects (animals, dolls, and everyday items) each with 5-6 representative images. To increase diversity, we apply the augmentation method in Section 4.1, generating 30 additional images per concept and forming the DreamBoothPlus dataset. Among the 30 objects of DreamBooth, we only augment 26, excluding four that pose challenges for text generation or require different fine-tuning parameters for cartoon-style content.

5.2 FITTING THE DISTANCE DISTRIBUTIONS

We use the DreamBoothPlus dataset to finetune a diffusion model (Dhariwal & Nichol, 2021; Nichol & Dhariwal, 2021) to fit the distance distribution p_{dis} (Details in Appendix D). We choose this model over more advanced architectures, such as the Stable Diffusion series (Podell et al., 2023; Rombach et al., 2022) or Flux, because it directly models $p(x)$ instead of $p(x | y)$, where x is the image and y is a label or prompt. Our goal is to employ a more principled model to illustrate our general adversarial attack method, rather than to optimize for the highest possible engineering performance.

5.3 CALCULATING THE DIFFERENCE BETWEEN KL DIVERGENCES

We empirically estimate the difference between two KL divergences,

$$\Delta := KL(p_{\text{dis}}^{(1)} \parallel p_{\text{vic}}) - KL(p_{\text{dis}}^{(2)} \parallel p_{\text{vic}}),$$

by using the Monte-Carlo method and the practical techniques introduced in Section 3.5 and Appendix B, and we denote this estimate by $\tilde{\Delta}$. Concretely, for each concept in DreamBoothPlus, we fine-tune a diffusion model on the entire concept to obtain $p_{\text{dis}}^{(1)}$. We then fine-tune a separate diffusion model on just one image to obtain $p_{\text{dis}}^{(2)}$. Next, we calculate the empirical difference $\tilde{\Delta}$ and find that $\tilde{\Delta} < 0$ for every concept. This strongly suggests that $\Delta < 0$, confirming our hypothesis from Section 3.5. The table in Appendix B summarizes the values of $\tilde{\Delta}$ for each concept.

5.4 GENERATING TARGETED ADVERSARIAL EXAMPLES

We evaluate the performance of the concept-based adversarial attack in a targeted adversarial attack setting, because targeted attacks are generally more difficult than untargeted attacks⁴. In our

³Although deterministic methods may yield different results when sampled multiple times, their variability does not stem from algorithmic design but rather from other sources of error.

⁴This is especially true for ImageNet classifiers, which must distinguish among 1,000 classes. In an untargeted attack, the goal is simply to prevent the victim classifier from assigning the adversarial sample to its

experiments, we compare NCF (Yuan et al., 2022), ACA (Chen et al., 2024b), DiffAttack (Chen et al., 2024a), and ProbAttack (Zhang et al., 2024b). We include NCF because it is the strongest color-based adversarial attack. Both ACA and DiffAttack apply adversarial gradients in the latent space induced by Stable Diffusion and DDIM, representing the state of the art in unrestricted adversarial attacks. As discussed earlier in Section 3, ProbAttack can be viewed as a special case of our approach when $|\mathcal{C}_{\text{ori}}| = 1$. For both ProbAttack and our approach, we set the number of samples M to 10. During the sample selection phase of the experiments, our method uses two strategies — a conservative strategy and an aggressive strategy (both described in Section 4.2) — denoted in the tables as OURS (CONS) and OURS (AGGR), respectively.

For each compared method, we conduct a white-box attack on the victim classifier (also referred to as the surrogate classifier) by generating adversarial samples based on it. Next, we feed these white-box-generated adversarial samples into other classifiers — a process known as a black-box attack. If these additional classifiers also classify the adversarial samples into the target class, the black-box attack is deemed successful, indicating transferability.

In our experiments, ResNet50 (He et al., 2016) is used as the victim classifier for white-box attacks. We measure transferability on VGG19 (Simonyan & Zisserman, 2015), ResNet152 (He et al., 2016), DenseNet161 (Huang et al., 2017), Inception V3 (Szegedy et al., 2016), EfficientNet B7 (Tan & Le, 2019), and on adversarially trained Inception V3 Adv (Kurakin et al., 2017), EfficientNet B7 Adv (Xie et al., 2020), and Ensemble IncRes V2 (Tramèr et al., 2018). We report both the white-box targeted attack success rate (on ResNet50) and the black-box transfer success rate (on the remaining models).

Table 1: Targeted attack success rates (%) on ImageNet classifiers. In the white-box setting, a targeted attack is counted as successful if the target class is ranked first. For transferability, we report top-5 success rates, counting an attack as successful if the target class is among the top 5 predictions (since top-1 success was uniformly low across all methods). See Appendix Q for full results.

	NCF	ACA	DiffAttack	ProbAttack	OURS (CONS)	OURS (AGGR)
White-box	Targeted-Top1					
ResNet 50	1.15	6.03	84.23	59.23	97.82	97.82
Transferability	Targeted-Top5					
VGG19	1.28	1.67	4.36	2.44	2.05	4.36
ResNet 152	1.41	1.92	8.33	3.33	2.82	8.72
DenseNet 161	1.41	2.05	7.44	3.97	3.85	11.54
Inception V3	0.90	1.41	3.08	2.56	1.28	4.74
EfficientNet B7	1.41	1.67	1.79	1.41	1.28	3.97
Adversarial Defence						
Inception V3 Adv	1.15	1.28	3.21	2.18	0.90	3.72
EfficientNet B7 Adv	0.26	1.15	2.05	2.31	1.67	6.41
Ensemble IncRes V2	0.77	1.28	2.69	1.92	0.77	5.00

For unrestricted adversarial examples, we must also check whether they preserve the original concept and remain undetectable to humans. Therefore, we measure similarity via a user study (Appendix F) and CLIP (Radford et al., 2021), and image quality using no-reference metrics (MUSIQ (Ke et al., 2021), TReS (Golestaneh et al., 2022), NIMA (Talebi & Milanfar, 2018), ARNIQA (Agnoletti et al., 2024), DBCNN (Zhang et al., 2020), and HyperIQA (Su et al., 2020)).

As ImageNet has 1,000 classes, it is impractical to evaluate them all. Therefore, we randomly select 30 target classes y_{tar} , listed in Appendix E. Since DreamBoothPlus contains 26 concepts, each method generates $26 \times 30 = 780$ adversarial examples. This scale is comparable to current popular approaches performing untargeted adversarial attacks on the ImageNet-Compatible dataset (Kurakin et al., 2018).

Table 1 presents the targeted attack success rates on ImageNet classifiers. Since the choice of aggressive or conservative strategy in the sample selection phase does not affect white-box performance, correct class. In contrast, a targeted attack requires the classifier to misclassify the adversarial sample exactly as the chosen target class y_{tar} .

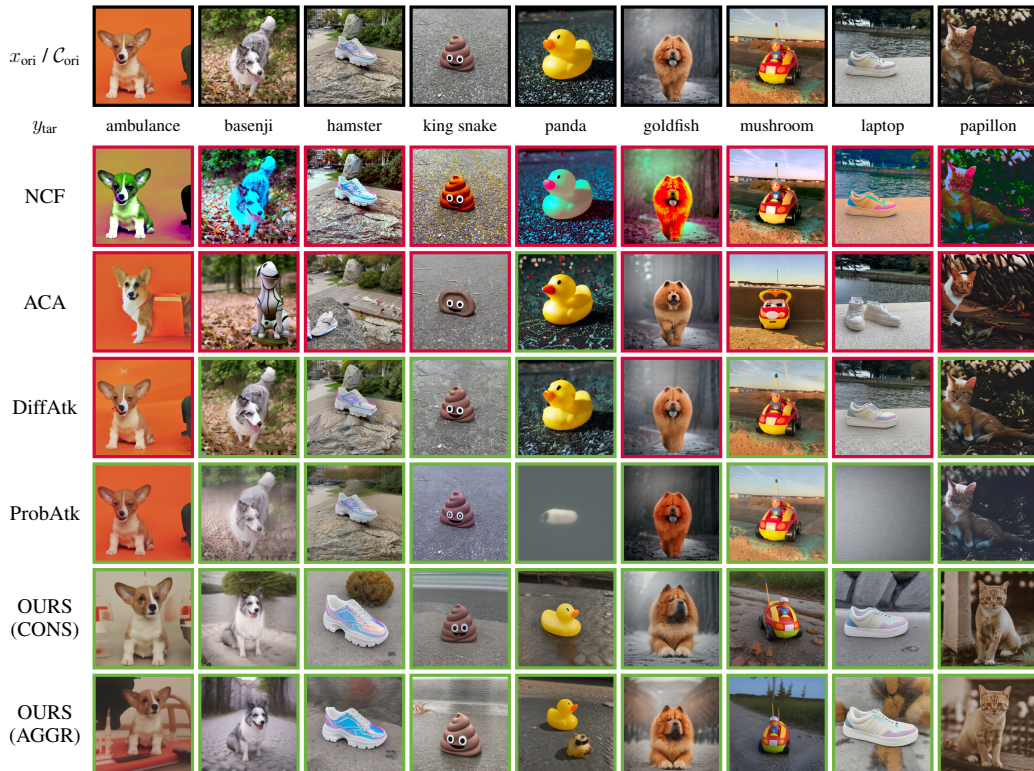


Figure 3: Qualitative comparison. (A **green** border indicates an example that successfully fools the classifier; **red** indicates failure.) See Appendix G for a more detailed qualitative analysis.

those rates are identical. Notably, the aggressive strategy achieves significantly higher transferability than other methods. While the conservative strategy leads to slightly lower transferability, it is still roughly comparable to the baseline methods. Please refer to Appendix Q for full results.

Table 2 reports the similarity between each adversarial sample and its original image, as well as the image quality of the generated examples. Both our aggressive and conservative strategies outperform the other methods in these metrics. Combined with the attack success rates in Table 1, our approach not only achieves higher success but also preserves the original concept C_{ori} more effectively. Figure 3 provides a qualitative comparison, showing how well our method maintains the original concept. Notably, DiffAttack generates images missing details, which aligns with its weaker image quality scores. For additional qualitative analysis, please refer to Appendix G.

Table 2: Quantitative comparison of similarity to the original images and no reference image quality metrics for unrestricted adversarial examples.

	Clean	NCF	ACA	DiffAttack	ProbAttack	OURS (CONS)	OURS (AGGR)
Similarity							
↑ User Study	N/A	0.1859	0.2808	0.7577	0.8041	0.9654	0.8808
↑ Avg. Clip Score	1.0	0.8728	0.7861	0.8093	0.8581	0.8283	0.8043
Image Quality							
↑ HyperIQ	0.7255	0.5075	0.6462	0.5551	0.6675	0.6947	0.6809
↑ DBCNN	0.6956	0.5096	0.6103	0.5294	0.6161	0.6572	0.6399
↑ ARNIQA	0.7667	0.5978	0.6879	0.6909	0.7009	0.7335	0.7154
↑ MUSIQ-AVA	4.3760	3.8135	4.2687	4.0734	4.3130	4.5305	4.5250
↑ NIMA-AVA	4.5595	3.7916	4.4511	4.0589	4.5168	4.7575	4.7401
↑ MUSIQ-KonIQ	65.0549	50.5022	59.0840	52.5399	58.1563	63.7486	62.2217
↑ TReS	93.2127	64.7050	85.8435	74.1167	84.3131	90.4488	88.0836

6 RELATED WORKS

To the best of our knowledge, no existing method constructs adversarial examples conditioned on an identity-level concept. The most closely related works are Song et al. (2018)’s, Dai et al. (2024)’s and Collins et al. (2025)’s. However, they treat a “class” (e.g., cat, dog, or truck) as the concept, which cannot precisely capture an individual identity. In our framework, we represent a concept through a distribution that could be learned from a set of images, allowing it to flexibly correspond to a single image (i.e. a set with size 1), an identity-level concept, or a class-level concept. By contrast, other unrestricted adversarial attack methods focus solely on generating adversarial examples from a single image: Xiao et al. (2018a) generate adversarial examples using GANs, Chen et al. (2023) employ diffusion models, and Laidlaw et al. (2020) impose a feature-space distance as a regularization term in the optimization objective. ACA (Chen et al., 2024b) and DiffAttack (Chen et al., 2024a) further apply the attack gradient directly in the DDIM latent space (Song et al., 2020). Color-based transformations have proven effective in preserving semantic content for untargeted attacks (Bhattad et al., 2020; Hosseini & Poovendran, 2018; Shamsabadi et al., 2020; Yuan et al., 2022; Zhao et al., 2020), yet they perform poorly in targeted scenarios (Chen et al., 2024a), a result confirmed by our experiments.

Unrestricted Adversarial Attack Method	Single-image	Identity-level Concept	Class-level Concept
Bhattad et al. (2020)	Yes	No	No
Hosseini & Poovendran (2018)	Yes	No	No
Colorfool (Shamsabadi et al., 2020)	Yes	No	No
Zhao et al. (2020)	Yes	No	No
NCF (Yuan et al., 2022)	Yes	No	No
ACA (Chen et al., 2024b)	Yes	No	No
DiffAttack (Chen et al., 2024a)	Yes	No	No
ProbAttack (Zhang et al., 2024b)	Yes	No	No
AdvGAN (Xiao et al., 2018a)	Yes	No	No
Xiao et al. (2018b)	Yes	No	No
Perceptual Adv. Attack (Laidlaw et al., 2020)	Yes	No	No
Song et al. (2018)	No	No	Yes
NatADiff (Collins et al., 2025)	No	No	Yes
AdvDiff (Dai et al., 2024)	No	No	Yes
AdvDiffuser Chen et al. (2023)	Yes	No	Yes
Ours: Concept-based Adv. Attack	Yes	Yes	Yes

Table 3: Comparison of unrestricted adversarial attack methods. Our method is the only one capable of performing adversarial attacks at the identity-level concept, while also supporting single-image and class-level concepts.

Our work directly inherited from Zhang et al. (2024b)’s probabilistic perspective, but we make a novel contribution by, for the first time, defining the distance distribution in adversarial attacks with respect to a distribution representing a concept rather than a single image. Although, operationally, our method appears to be a straightforward extension — replacing the single-image-centered distribution $p_{\text{dis}}(\cdot | x_{\text{ori}})$ with a concept-centered distribution $p_{\text{dis}}(\cdot | C_{\text{ori}})$ (as in the difference between (2) and (3)) — we rigorously demonstrate, both theoretically and empirically, why this seemingly simple generalization is remarkably effective.

7 CONCLUSIONS

The essence of adversarial attacks is to create examples that are imperceptible to humans yet harmful to computational systems. Our work demonstrates that in an era of powerful generative models, creating an adversarial example from scratch — one that humans perceive as conceptually correct — can be more flexible, more realistic, and ultimately more potent than simply perturbing a single image. Leveraging modern generative models, adversarial noise can be concealed in subtle changes to viewpoint, pose, or background, making it exceedingly difficult to detect. We believe that our concept-based adversarial attack heralds the future of adversarial attacks, posing new challenges to the field of AI security. Defending against such threats will be crucial for advancing AI security research.

ACKNOWLEDGMENTS

This work was supported by the Engineering and Physical Sciences Research Council (EPSRC) through the AI Hub in Generative Models (EP/Y028805/1).

AZ and SK were funded by the UKRI AI Hub in Generative Models (EP/Y028805/1). SM was supported by the UKRI AI Programme Grant (EP/Y028856/1). AZ also acknowledges support from a personal grant provided by Mrs. Yanshu Wu. SK was additionally supported by the Research Council of Finland (Flagship Programme: Finnish Center for Artificial Intelligence FCAI, 359207) and the UKRI Turing AI World-Leading Researcher Fellowship (EP/W002973/1).

ETHICS STATEMENT

This work introduces a new class of adversarial attacks that operate at the concept level. While our primary goal is to advance scientific understanding of adversarial robustness and stimulate the development of stronger defenses, we acknowledge the potential for malicious misuse. In particular, concept-based adversarial attacks could be exploited to evade security-sensitive image classifiers or to manipulate systems deployed in safety-critical applications.

To mitigate these risks, we have:

- Released all code and data strictly for research purposes, under licenses that encourage responsible use.
- Discussed mitigation strategies in Appendix L, including adversarial training, AI-generated content detection, and hybrid defenses.

We emphasize that the broader impact (Appendix M) of this work depends on the research community’s response. By exposing vulnerabilities of current classifiers, we aim to encourage the development of more robust and trustworthy AI systems. We strongly discourage any use of this research for harmful purposes.

REPRODUCIBILITY STATEMENT

We have taken several steps to ensure the reproducibility of our work:

- **Code and models:** We provide the full source code, including scripts for dataset preparation, model fine-tuning, and adversarial example generation, at <https://github.com/andiac/ConceptAdv>. All hyperparameters and training details are specified in the code repository.
- **Datasets:** Our experiments are based on the DreamBooth dataset (Ruiz et al., 2023), which is publicly available under a CC-BY-4.0 license. We also describe our augmentation procedure using SDXL and LoRA in Section 4.1, and provide scripts for generating data (DreamBoothPlus) as part of our code repo.
- **Hyperparameters:** Fine-tuning settings for both SDXL LoRA and diffusion models are detailed in Appendix D. For sampling and evaluation, we report the number of generated adversarial examples, sampling strategies, and evaluation metrics in Sections 4-5.
- **Theoretical results:** Proofs of all theorems are included in Appendix A, and additional details on KL divergence estimation are in Appendix B.
- **Compute resources:** We report hardware specifications and training times in Appendix I to allow others to reproduce our experiments with similar resources.

We believe these resources provide sufficient detail for reproducing both our theoretical and empirical results.

REFERENCES

- Lorenzo Agnolucci, Leonardo Galteri, Marco Bertini, and Alberto Del Bimbo. Arniqa: Learning distortion manifold for image quality assessment. In *Proceedings of the IEEE/CVF Winter Conference on Applications of Computer Vision*, pp. 189–198, 2024.
- Anand Bhattad, Min Jin Chong, Kaizhao Liang, Bo Li, and David A. Forsyth. Unrestricted adversarial examples via semantic manipulation. In *8th International Conference on Learning Representations, ICLR 2020, Addis Ababa, Ethiopia, April 26-30, 2020*. OpenReview.net, 2020. URL https://openreview.net/forum?id=Sye_OgHFwH.
- Battista Biggio and Fabio Roli. Wild patterns: Ten years after the rise of adversarial machine learning. In *Proceedings of the 2018 ACM SIGSAC Conference on Computer and Communications Security*, pp. 2154–2156, 2018.
- Yuri Burda, Roger Grosse, and Ruslan Salakhutdinov. Importance weighted autoencoders. *arXiv preprint arXiv:1509.00519*, 2015.
- Nicholas Carlini and David Wagner. Towards evaluating the robustness of neural networks. In *2017 IEEE Symposium on Security and Privacy (SP)*, pp. 39–57. Ieee, 2017.
- Jianqi Chen, Hao Chen, Keyan Chen, Yilan Zhang, Zhengxia Zou, and Zhenwei Shi. Diffusion models for imperceptible and transferable adversarial attack. *IEEE Transactions on Pattern Analysis and Machine Intelligence*, pp. 1–17, 2024a. doi: 10.1109/TPAMI.2024.3480519.
- Xinquan Chen, Xitong Gao, Juanjuan Zhao, Kejiang Ye, and Cheng-Zhong Xu. Advdiffuser: Natural adversarial example synthesis with diffusion models. In *Proceedings of the IEEE/CVF International Conference on Computer Vision*, pp. 4562–4572, 2023.
- Zhaoyu Chen, Bo Li, Shuang Wu, Kaixun Jiang, Shouhong Ding, and Wenqiang Zhang. Content-based unrestricted adversarial attack. *Advances in Neural Information Processing Systems*, 36, 2024b.
- Max Collins, Jordan Vice, Tim French, and Ajmal Mian. Natadiff: Adversarial boundary guidance for natural adversarial diffusion. *arXiv preprint arXiv:2505.20934*, 2025.
- Francesco Croce, Maksym Andriushchenko, Vikash Sehwal, Edoardo DeBenedetti, Nicolas Flammarion, Mung Chiang, Prateek Mittal, and Matthias Hein. Robustbench: a standardized adversarial robustness benchmark. *arXiv preprint arXiv:2010.09670*, 2020.
- Xuelong Dai, Kaisheng Liang, and Bin Xiao. Advdiff: Generating unrestricted adversarial examples using diffusion models. In *European Conference on Computer Vision*, pp. 93–109. Springer, 2024.
- Nilesh Dalvi, Pedro Domingos, Mausam, Sumit Sanghai, and Deepak Verma. Adversarial classification. In *Proceedings of the tenth ACM SIGKDD international conference on Knowledge discovery and data mining*, pp. 99–108, 2004.
- Prafulla Dhariwal and Alexander Quinn Nichol. Diffusion models beat gans on image synthesis. In Marc’Aurelio Ranzato, Alina Beygelzimer, Yann N. Dauphin, Percy Liang, and Jennifer Wortman Vaughan (eds.), *Advances in Neural Information Processing Systems 34: Annual Conference on Neural Information Processing Systems 2021, NeurIPS 2021, December 6-14, 2021, virtual*, pp. 8780–8794, 2021. URL <https://proceedings.neurips.cc/paper/2021/hash/49ad23d1ec9fa4bd8d77d02681df5cfa-Abstract.html>.
- Yinpeng Dong, Qi-An Fu, Xiao Yang, Wenzhao Xiang, Tianyu Pang, Hang Su, Jun Zhu, Jiayu Tang, Yuefeng Chen, XiaoFeng Mao, et al. Adversarial attacks on ml defense models competition. *arXiv preprint arXiv:2110.08042*, 2021.
- S Alireza Golestaneh, Saba Dadsetan, and Kris M Kitani. No-reference image quality assessment via transformers, relative ranking, and self-consistency. In *Proceedings of the IEEE/CVF winter conference on applications of computer vision*, pp. 1220–1230, 2022.

- Ian J. Goodfellow, Jonathon Shlens, and Christian Szegedy. Explaining and harnessing adversarial examples. In Yoshua Bengio and Yann LeCun (eds.), *3rd International Conference on Learning Representations, ICLR 2015, San Diego, CA, USA, May 7-9, 2015, Conference Track Proceedings*, 2015. URL <http://arxiv.org/abs/1412.6572>.
- Martin Gubri, Maxime Cordy, Mike Papadakis, Yves Le Traon, and Koushik Sen. Lgv: Boosting adversarial example transferability from large geometric vicinity. In *European Conference on Computer Vision*, pp. 603–618. Springer, 2022.
- Kaiming He, Xiangyu Zhang, Shaoqing Ren, and Jian Sun. Deep residual learning for image recognition. In *2016 IEEE Conference on Computer Vision and Pattern Recognition, CVPR 2016, Las Vegas, NV, USA, June 27-30, 2016*, pp. 770–778. IEEE Computer Society, 2016. doi: 10.1109/CVPR.2016.90. URL <https://doi.org/10.1109/CVPR.2016.90>.
- Geoffrey E Hinton. Training products of experts by minimizing contrastive divergence. *Neural computation*, 14(8):1771–1800, 2002.
- Jonathan Ho, Ajay Jain, and Pieter Abbeel. Denoising diffusion probabilistic models. In Hugo Larochelle, Marc’Aurelio Ranzato, Raia Hadsell, Maria-Florina Balcan, and Hsuan-Tien Lin (eds.), *Advances in Neural Information Processing Systems 33: Annual Conference on Neural Information Processing Systems 2020, NeurIPS 2020, December 6-12, 2020, virtual*, 2020. URL <https://proceedings.neurips.cc/paper/2020/hash/4c5bcfec8584af0d967f1ab10179ca4b-Abstract.html>.
- Hossein Hosseini and Radha Poovendran. Semantic adversarial examples. In *Proceedings of the IEEE Conference on Computer Vision and Pattern Recognition Workshops*, pp. 1614–1619, 2018.
- Edward J. Hu, Yelong Shen, Phillip Wallis, Zeyuan Allen-Zhu, Yuanzhi Li, Shean Wang, Lu Wang, and Weizhu Chen. Lora: Low-rank adaptation of large language models. In *The Tenth International Conference on Learning Representations, ICLR 2022, Virtual Event, April 25-29, 2022*. OpenReview.net, 2022. URL <https://openreview.net/forum?id=nZeVKeeFYf9>.
- Gao Huang, Zhuang Liu, Laurens van der Maaten, and Kilian Q. Weinberger. Densely connected convolutional networks. In *2017 IEEE Conference on Computer Vision and Pattern Recognition, CVPR 2017, Honolulu, HI, USA, July 21-26, 2017*, pp. 2261–2269. IEEE Computer Society, 2017. doi: 10.1109/CVPR.2017.243. URL <https://doi.org/10.1109/CVPR.2017.243>.
- Aaron Hurst, Adam Lerer, Adam P Goucher, Adam Perelman, Aditya Ramesh, Aidan Clark, AJ Ostrow, Akila Welihinda, Alan Hayes, Alec Radford, et al. Gpt-4o system card. *arXiv preprint arXiv:2410.21276*, 2024.
- Junjie Ke, Qifei Wang, Yilin Wang, Peyman Milanfar, and Feng Yang. Musiq: Multi-scale image quality transformer. In *Proceedings of the IEEE/CVF international conference on computer vision*, pp. 5148–5157, 2021.
- Diederik P Kingma, Max Welling, et al. Auto-encoding variational bayes, 2013.
- Alexey Kurakin, Ian J. Goodfellow, and Samy Bengio. Adversarial machine learning at scale. In *5th International Conference on Learning Representations, ICLR 2017, Toulon, France, April 24-26, 2017, Conference Track Proceedings*. OpenReview.net, 2017. URL <https://openreview.net/forum?id=BJm4T4Kgx>.
- Alexey Kurakin, Ian J Goodfellow, and Samy Bengio. Adversarial examples in the physical world. In *Artificial intelligence safety and security*, pp. 99–112. Chapman and Hall/CRC, 2018.
- Cassidy Laidlaw, Sahil Singla, and Soheil Feizi. Perceptual adversarial robustness: Defense against unseen threat models. *arXiv preprint arXiv:2006.12655*, 2020.
- Andrew Lamperski. Projected stochastic gradient langevin algorithms for constrained sampling and non-convex learning. In *Conference on Learning Theory*, pp. 2891–2937. PMLR, 2021.
- Yann LeCun, Sumit Chopra, Raia Hadsell, M Ranzato, Fugie Huang, et al. A tutorial on energy-based learning. *Predicting structured data*, 1(0), 2006.

- Daniel Lowd and Christopher Meek. Adversarial learning. In *Proceedings of the eleventh ACM SIGKDD international conference on Knowledge discovery in data mining*, pp. 641–647, 2005a.
- Daniel Lowd and Christopher Meek. Good word attacks on statistical spam filters. In *CEAS*, volume 2005, 2005b.
- Aleksander Madry, Aleksandar Makelov, Ludwig Schmidt, Dimitris Tsipras, and Adrian Vladu. Towards deep learning models resistant to adversarial attacks. In *6th International Conference on Learning Representations, ICLR 2018, Vancouver, BC, Canada, April 30 - May 3, 2018, Conference Track Proceedings*. OpenReview.net, 2018. URL <https://openreview.net/forum?id=rJzIBfZAb>.
- Eric T. Nalisnick, Akihiro Matsukawa, Yee Whye Teh, Dilan Görür, and Balaji Lakshminarayanan. Do deep generative models know what they don’t know? In *7th International Conference on Learning Representations, ICLR 2019, New Orleans, LA, USA, May 6-9, 2019*. OpenReview.net, 2019. URL <https://openreview.net/forum?id=HlxwNhCcYm>.
- Alexander Quinn Nichol and Prafulla Dhariwal. Improved denoising diffusion probabilistic models. In Marina Meila and Tong Zhang (eds.), *Proceedings of the 38th International Conference on Machine Learning, ICML 2021, 18-24 July 2021, Virtual Event*, volume 139 of *Proceedings of Machine Learning Research*, pp. 8162–8171. PMLR, 2021. URL <http://proceedings.mlr.press/v139/nichol21a.html>.
- Dustin Podell, Zion English, Kyle Lacey, Andreas Blattmann, Tim Dockhorn, Jonas Müller, Joe Penna, and Robin Rombach. Sdxl: Improving latent diffusion models for high-resolution image synthesis. *arXiv preprint arXiv:2307.01952*, 2023.
- Eleonora Poeta, Gabriele Ciravegna, Eliana Pastor, Tania Cerquitelli, and Elena Baralis. Concept-based explainable artificial intelligence: A survey. *ACM Computing Surveys*, 2023.
- Alec Radford, Jong Wook Kim, Chris Hallacy, Aditya Ramesh, Gabriel Goh, Sandhini Agarwal, Girish Sastry, Amanda Askell, Pamela Mishkin, Jack Clark, et al. Learning transferable visual models from natural language supervision. In *International conference on machine learning*, pp. 8748–8763. PmLR, 2021.
- Robin Rombach, Andreas Blattmann, Dominik Lorenz, Patrick Esser, and Björn Ommer. High-resolution image synthesis with latent diffusion models. In *Proceedings of the IEEE/CVF conference on computer vision and pattern recognition*, pp. 10684–10695, 2022.
- Nataniel Ruiz, Yuanzhen Li, Varun Jampani, Yael Pritch, Michael Rubinstein, and Kfir Aberman. Dreambooth: Fine tuning text-to-image diffusion models for subject-driven generation. In *Proceedings of the IEEE/CVF Conference on Computer Vision and Pattern Recognition*, pp. 22500–22510, 2023.
- Shibani Santurkar, Andrew Ilyas, Dimitris Tsipras, Logan Engstrom, Brandon Tran, and Aleksander Madry. Image synthesis with a single (robust) classifier. In Hanna M. Wallach, Hugo Larochelle, Alina Beygelzimer, Florence d’Alché-Buc, Emily B. Fox, and Roman Garnett (eds.), *Advances in Neural Information Processing Systems 32: Annual Conference on Neural Information Processing Systems 2019, NeurIPS 2019, December 8-14, 2019, Vancouver, BC, Canada*, pp. 1260–1271, 2019. URL <https://proceedings.neurips.cc/paper/2019/hash/6f2268bd1d3d3ebaabb04d6b5d099425-Abstract.html>.
- Ali Shahin Shamsabadi, Ricardo Sánchez-Matilla, and Andrea Cavallaro. Colorfool: Semantic adversarial colorization. In *2020 IEEE/CVF Conference on Computer Vision and Pattern Recognition, CVPR 2020, Seattle, WA, USA, June 13-19, 2020*, pp. 1148–1157. IEEE, 2020. doi: 10.1109/CVPR42600.2020.00123. URL <https://doi.org/10.1109/CVPR42600.2020.00123>.
- Karen Simonyan and Andrew Zisserman. Very deep convolutional networks for large-scale image recognition. In Yoshua Bengio and Yann LeCun (eds.), *3rd International Conference on Learning Representations, ICLR 2015, San Diego, CA, USA, May 7-9, 2015, Conference Track Proceedings*, 2015. URL <http://arxiv.org/abs/1409.1556>.

- Jiaming Song, Chenlin Meng, and Stefano Ermon. Denoising diffusion implicit models. *arXiv preprint arXiv:2010.02502*, 2020.
- Yang Song and Stefano Ermon. Generative modeling by estimating gradients of the data distribution. *Advances in neural information processing systems*, 32, 2019.
- Yang Song, Rui Shu, Nate Kushman, and Stefano Ermon. Constructing unrestricted adversarial examples with generative models. In Samy Bengio, Hanna M. Wallach, Hugo Larochelle, Kristen Grauman, Nicolò Cesa-Bianchi, and Roman Garnett (eds.), *Advances in Neural Information Processing Systems 31: Annual Conference on Neural Information Processing Systems 2018, NeurIPS 2018, December 3-8, 2018, Montréal, Canada*, pp. 8322–8333, 2018. URL <https://proceedings.neurips.cc/paper/2018/hash/8cea559c47e4fbdb73b23e0223d04e79-Abstract.html>.
- Shaolin Su, Qingsen Yan, Yu Zhu, Cheng Zhang, Xin Ge, Jinqiu Sun, and Yanning Zhang. Blindly assess image quality in the wild guided by a self-adaptive hyper network. In *Proceedings of the IEEE/CVF conference on computer vision and pattern recognition*, pp. 3667–3676, 2020.
- Christian Szegedy, Wojciech Zaremba, Ilya Sutskever, Joan Bruna, Dumitru Erhan, Ian J. Goodfellow, and Rob Fergus. Intriguing properties of neural networks. In Yoshua Bengio and Yann LeCun (eds.), *2nd International Conference on Learning Representations, ICLR 2014, Banff, AB, Canada, April 14-16, 2014, Conference Track Proceedings*, 2014. URL <http://arxiv.org/abs/1312.6199>.
- Christian Szegedy, Vincent Vanhoucke, Sergey Ioffe, Jonathon Shlens, and Zbigniew Wojna. Rethinking the inception architecture for computer vision. In *2016 IEEE Conference on Computer Vision and Pattern Recognition, CVPR 2016, Las Vegas, NV, USA, June 27-30, 2016*, pp. 2818–2826. IEEE Computer Society, 2016. doi: 10.1109/CVPR.2016.308. URL <https://doi.org/10.1109/CVPR.2016.308>.
- Hossein Talebi and Peyman Milanfar. Nima: Neural image assessment. *IEEE transactions on image processing*, 27(8):3998–4011, 2018.
- Mingxing Tan and Quoc V. Le. Efficientnet: Rethinking model scaling for convolutional neural networks. In Kamalika Chaudhuri and Ruslan Salakhutdinov (eds.), *Proceedings of the 36th International Conference on Machine Learning, ICML 2019, 9-15 June 2019, Long Beach, California, USA*, volume 97 of *Proceedings of Machine Learning Research*, pp. 6105–6114. PMLR, 2019. URL <http://proceedings.mlr.press/v97/tan19a.html>.
- Florian Tramèr, Alexey Kurakin, Nicolas Papernot, Ian J. Goodfellow, Dan Boneh, and Patrick D. McDaniel. Ensemble adversarial training: Attacks and defenses. In *6th International Conference on Learning Representations, ICLR 2018, Vancouver, BC, Canada, April 30 - May 3, 2018, Conference Track Proceedings*. OpenReview.net, 2018. URL <https://openreview.net/forum?id=rkZvSe-RZ>.
- Xiaosen Wang and Kun He. Enhancing the transferability of adversarial attacks through variance tuning. In *Proceedings of the IEEE/CVF conference on computer vision and pattern recognition*, pp. 1924–1933, 2021.
- Zhixiang Wang, Xiaosen Wang, Bo Wang, Siheng Chen, Zhibo Wang, Xingjun Ma, and Yu-Gang Jiang. Diffpatch: Generating customizable adversarial patches using diffusion models. *arXiv preprint arXiv:2412.01440*, 2024.
- Chaowei Xiao, Bo Li, Jun-Yan Zhu, Warren He, Mingyan Liu, and Dawn Song. Generating adversarial examples with adversarial networks. *arXiv preprint arXiv:1801.02610*, 2018a.
- Chaowei Xiao, Jun-Yan Zhu, Bo Li, Warren He, Mingyan Liu, and Dawn Song. Spatially transformed adversarial examples. In *6th International Conference on Learning Representations, ICLR 2018, Vancouver, BC, Canada, April 30 - May 3, 2018, Conference Track Proceedings*. OpenReview.net, 2018b. URL <https://openreview.net/forum?id=HyydRMZC->.

- Cihang Xie, Mingxing Tan, Boqing Gong, Jiang Wang, Alan L. Yuille, and Quoc V. Le. Adversarial examples improve image recognition. In *2020 IEEE/CVF Conference on Computer Vision and Pattern Recognition, CVPR 2020, Seattle, WA, USA, June 13-19, 2020*, pp. 816–825. IEEE, 2020. doi: 10.1109/CVPR42600.2020.00090. URL <https://doi.org/10.1109/CVPR42600.2020.00090>.
- Shengming Yuan, Qilong Zhang, Lianli Gao, Yaya Cheng, and Jingkuan Song. Natural color fool: Towards boosting black-box unrestricted attacks. *Advances in Neural Information Processing Systems*, 35:7546–7560, 2022.
- Andi Zhang, Tim Z Xiao, Weiyang Liu, Robert Bamler, and Damon Wischik. Your fine-tuned large language model is already a powerful out-of-distribution detector. *arXiv preprint arXiv:2404.08679*, 2024a.
- Andi Zhang, Mingtian Zhang, and Damon Wischik. Constructing semantics-aware adversarial examples with a probabilistic perspective. *Advances in Neural Information Processing Systems*, 37:136259–136285, 2024b.
- Weixia Zhang, Kede Ma, Jia Yan, Dexiang Deng, and Zhou Wang. Blind image quality assessment using a deep bilinear convolutional neural network. *IEEE Transactions on Circuits and Systems for Video Technology*, 30(1):36–47, 2020.
- Zhengyu Zhao, Zhuoran Liu, and Martha A. Larson. Adversarial color enhancement: Generating unrestricted adversarial images by optimizing a color filter. In *31st British Machine Vision Conference 2020, BMVC 2020, Virtual Event, UK, September 7-10, 2020*. BMVA Press, 2020. URL <https://www.bmvc2020-conference.com/assets/papers/0099.pdf>.
- Yao Zhu, Jiacheng Ma, Jiacheng Sun, Zewei Chen, Rongxin Jiang, Yaowu Chen, and Zhenguo Li. Towards understanding the generative capability of adversarially robust classifiers. In *Proceedings of the IEEE/CVF International Conference on Computer Vision*, pp. 7728–7737, 2021.
- Yao Zhu, Yuefeng Chen, Xiaodan Li, Kejiang Chen, Yuan He, Xiang Tian, Bolun Zheng, Yaowu Chen, and Qingming Huang. Toward understanding and boosting adversarial transferability from a distribution perspective. *IEEE Transactions on Image Processing*, 31:6487–6501, 2022.

APPENDIX

A PROOF OF THE THEOREMS

Theorem 1. Let p be a probability distribution and q be a Gibbs distribution of the form

$$q(x) = \frac{\exp(-\beta D(x, \mu))}{Z(\beta)},$$

where $Z(\beta)$ is the normalizing constant, μ is a constant and D is a distance function. Then $KL(p \parallel q)$ is a increasing function of β whenever $\mathbb{E}_{X \sim p}[D(X, \mu)] > \mathbb{E}_{X \sim q}[D(X, \mu)]$.

Proof. According to the definition of KL divergence, we have

$$KL(p \parallel q) = \int p(x) \log \frac{p(x)}{q(x)} dx = \int p(x) \log p(x) dx - \int p(x) \log q(x) dx$$

Since $\int p(x) \log p(x) dx$ is independent of β , we can treat it as a constant. Let us denote the β -dependent component as $f(\beta)$, which gives us

$$\begin{aligned} f(\beta) &= - \int p(x) \log q(x) dx \\ &= - \int p(x) [-\beta D(x, \mu) - \log Z(\beta)] dx \\ &= \int p(x) \beta D(x, \mu) dx + \log Z(\beta) \int p(x) dx \\ &= \mathbb{E}_{X \sim p}[\beta D(X, \mu)] + \log Z(\beta) \end{aligned}$$

Taking the derivative with respect to β , we obtain

$$\begin{aligned} \frac{d}{d\beta} f(\beta) &= \mathbb{E}_{X \sim p}[D(X, \mu)] + \frac{1}{Z(\beta)} \frac{dZ(\beta)}{d\beta} \\ &= \mathbb{E}_{X \sim p}[D(X, \mu)] + \frac{1}{Z(\beta)} \int \frac{d \exp(-\beta D(X, \mu))}{d\beta} dx \\ &= \mathbb{E}_{X \sim p}[D(X, \mu)] + \frac{1}{Z(\beta)} \int -D(X, \mu) \exp(-\beta D(X, \mu)) dx \\ &= \mathbb{E}_{X \sim p}[D(X, \mu)] - \mathbb{E}_{X \sim q}[D(X, \mu)] \end{aligned}$$

Therefore, when $\mathbb{E}_{X \sim p}[D(X, \mu)] > \mathbb{E}_{X \sim q}[D(X, \mu)]$, the derivative becomes positive. This implies that both $f(\beta)$ and consequently $KL(p \parallel q)$ increase as β increases. \square

Theorem 2. Let $p_{dis}^{(1)} = p_{dis}(\cdot \mid \mathcal{C}_{ori}^{(1)})$ and $p_{dis}^{(2)} = p_{dis}(\cdot \mid \mathcal{C}_{ori}^{(2)})$ be two distance distributions, and let $p_{vic}(\cdot \mid y_{tar})$ be the victim distribution corresponding to a victim classifier $p(y_{tar} \mid x)$. Then, the difference

$$\Delta = KL(p_{dis}^{(1)} \parallel p_{vic}) - KL(p_{dis}^{(2)} \parallel p_{vic})$$

is given by

$$\Delta = \mathbb{E}_{X \sim p_{dis}^{(1)}} [\log p_{dis}^{(1)}(X) - c \log p(y_{tar} \mid X)] - \mathbb{E}_{X \sim p_{dis}^{(2)}} [\log p_{dis}^{(2)}(X) - c \log p(y_{tar} \mid X)].$$

Proof. Recall that for distributions p and q on the same space, the Kullback–Leibler (KL) divergence is

$$KL(p \parallel q) = \mathbb{E}_{X \sim p} [\log p(X) - \log q(X)].$$

Hence, for $p_{dis}(\cdot \mid \mathcal{C}_{ori})$ and $p_{vic}(\cdot \mid y_{tar})$,

$$KL(p_{dis}(\cdot \mid \mathcal{C}_{ori}) \parallel p_{vic}(\cdot \mid y_{tar})) = \mathbb{E}_{X \sim p_{dis}(\cdot \mid \mathcal{C}_{ori})} [\log p_{dis}(X \mid \mathcal{C}_{ori}) - \log p_{vic}(X \mid y_{tar})].$$

Given that the victim distribution is proportional to

$$p_{\text{vic}}(x | y_{\text{tar}}) \propto \exp(-c f(x, y_{\text{tar}})),$$

where $f(x, y_{\text{tar}})$ is the cross-entropy loss, i.e. $f(x, y_{\text{tar}}) = -\log p(y_{\text{tar}} | x)$. Thus we can write

$$p_{\text{vic}}(x | y_{\text{tar}}) = \frac{\exp(-c f(x, y_{\text{tar}}))}{\int \exp(-c f(x, y_{\text{tar}})) dx}.$$

Let $Z := \int \exp(-c f(x, y_{\text{tar}})) dx$. Then

$$\log p_{\text{vic}}(X | y_{\text{tar}}) = \log \exp(-c f(X, y_{\text{tar}})) - \log Z = -c f(X, y_{\text{tar}}) - \log Z.$$

Therefore,

$$KL(p_{\text{dis}}(\cdot | \mathcal{C}_{\text{ori}}) \| p_{\text{vic}}(\cdot | y_{\text{tar}})) = \mathbb{E}_{X \sim p_{\text{dis}}(\cdot | \mathcal{C}_{\text{ori}})} [\log p_{\text{dis}}(X | \mathcal{C}_{\text{ori}}) + c f(X, y_{\text{tar}})] + \log Z.$$

Since $f(x, y_{\text{tar}}) = -\log p(y_{\text{tar}} | x)$, we get

$$c \mathbb{E}_{X \sim p_{\text{dis}}(\cdot | \mathcal{C}_{\text{ori}})} [f(X, y_{\text{tar}})] = -c \mathbb{E}_{X \sim p_{\text{dis}}(\cdot | \mathcal{C}_{\text{ori}})} [\log p(y_{\text{tar}} | X)].$$

Hence

$$KL(p_{\text{dis}}(\cdot | \mathcal{C}_{\text{ori}}) \| p_{\text{vic}}(\cdot | y_{\text{tar}})) = \mathbb{E}_{X \sim p_{\text{dis}}(\cdot | \mathcal{C}_{\text{ori}})} [\log p_{\text{dis}}(X | \mathcal{C}_{\text{ori}}) - c \log p(y_{\text{tar}} | X)] + \log Z.$$

Now take two such distributions, $p_{\text{dis}}^{(1)}$ and $p_{\text{dis}}^{(2)}$. Because $\log Z$ does not depend on which $p_{\text{dis}}(\cdot | \mathcal{C}_{\text{ori}})$ we use, it cancels when we form the difference:

$$\begin{aligned} \Delta &= KL(p_{\text{dis}}^{(1)} \| p_{\text{vic}}) - KL(p_{\text{dis}}^{(2)} \| p_{\text{vic}}) \\ &= \left(\mathbb{E}_{X \sim p_{\text{dis}}^{(1)}} [\log p_{\text{dis}}^{(1)}(X) - c \log p(y_{\text{tar}} | X)] + \log Z \right) \\ &\quad - \left(\mathbb{E}_{X \sim p_{\text{dis}}^{(2)}} [\log p_{\text{dis}}^{(2)}(X) - c \log p(y_{\text{tar}} | X)] + \log Z \right) \\ &= \mathbb{E}_{X \sim p_{\text{dis}}^{(1)}} [\log p_{\text{dis}}^{(1)}(X) - c \log p(y_{\text{tar}} | X)] - \mathbb{E}_{X \sim p_{\text{dis}}^{(2)}} [\log p_{\text{dis}}^{(2)}(X) - c \log p(y_{\text{tar}} | X)], \end{aligned}$$

which is precisely the claimed result. \square

B PRACTICAL STRATEGIES FOR KL DIVERGENCE ESTIMATION

B.1 COMMON RANDOM NUMBERS

In practice, our distance distributions $p_{\text{dis}}^{(1)}$ and $p_{\text{dis}}^{(2)}$ are instantiated by diffusion models: each image X is generated from noise ϵ via a generator \mathcal{G} . We write $X = \mathcal{G}^{(1)}(\epsilon)$ to indicate that X is sampled from $p_{\text{dis}}^{(1)}$, and $X = \mathcal{G}^{(2)}(\epsilon)$ to indicate that X is sampled from $p_{\text{dis}}^{(2)}$. In this common-noise setup, the difference in KL divergences becomes

$$\Delta = \mathbb{E}_{\epsilon} \left[\log p_{\text{dis}}^{(1)}(\mathcal{G}^{(1)}(\epsilon)) - c \log p(y_{\text{tar}} | \mathcal{G}^{(1)}(\epsilon)) - \log p_{\text{dis}}^{(2)}(\mathcal{G}^{(2)}(\epsilon)) + c \log p(y_{\text{tar}} | \mathcal{G}^{(2)}(\epsilon)) \right]. \quad (4)$$

B.2 LIKELIHOOD CORRECTION

We posit a probabilistic model p_{share} that captures the non-semantic, shared features of the images. Specifically, we assume that for samples X drawn from $p_{\text{dis}}^{(1)}$ and $p_{\text{dis}}^{(2)}$, the expected values $\mathbb{E}_{X \sim p_{\text{dis}}^{(1)}} [\log p_{\text{share}}(X)]$ and $\mathbb{E}_{X \sim p_{\text{dis}}^{(2)}} [\log p_{\text{share}}(X)]$ are equal. This assumption is reasonable because the two distributions, in principle, can generate images sharing the same non-semantic details, differing only in their semantic content.

Then, under our diffusion-model instantiation, we have

$$\mathbb{E}_{X \sim p_{\text{dis}}^{(1)}} [\log p_{\text{share}}(X)] = \mathbb{E}_{X \sim p_{\text{dis}}^{(2)}} [\log p_{\text{share}}(X)] \Rightarrow \mathbb{E}_{\epsilon} [\log p_{\text{share}}(\mathcal{G}^{(1)}(\epsilon)) - \log p_{\text{share}}(\mathcal{G}^{(2)}(\epsilon))] = 0$$

for Δ , following equation 4, we have the equations:

$$\begin{aligned} \Delta &= \mathbb{E}_\epsilon \left[\log p_{\text{dis}}^{(1)}(\mathcal{G}^{(1)}(\epsilon)) - c \log p(y_{\text{tar}} | \mathcal{G}^{(1)}(\epsilon)) - \log p_{\text{dis}}^{(2)}(\mathcal{G}^{(2)}(\epsilon)) + c \log p(y_{\text{tar}} | \mathcal{G}^{(2)}(\epsilon)) \right] \\ &\quad - \mathbb{E}_\epsilon \left[\log p_{\text{share}}(\mathcal{G}^{(1)}(\epsilon)) - \log p_{\text{share}}(\mathcal{G}^{(2)}(\epsilon)) \right] \\ &= \mathbb{E}_\epsilon \left[\log p_{\text{dis}}^{(1)}(\mathcal{G}^{(1)}(\epsilon)) - \log p_{\text{share}}(\mathcal{G}^{(1)}(\epsilon)) - c \log p(y_{\text{tar}} | \mathcal{G}^{(1)}(\epsilon)) \right. \\ &\quad \left. - \log p_{\text{dis}}^{(2)}(\mathcal{G}^{(2)}(\epsilon)) + \log p_{\text{share}}(\mathcal{G}^{(2)}(\epsilon)) + c \log p(y_{\text{tar}} | \mathcal{G}^{(2)}(\epsilon)) \right] \end{aligned}$$

In practice, however, the assumption $\mathbb{E}_{X \sim p_{\text{dis}}^{(1)}}[p_{\text{share}}(X)] = \mathbb{E}_{X \sim p_{\text{dis}}^{(2)}}[p_{\text{share}}(X)]$ may not hold perfectly, due to differences in model capacity, finetuning steps, and other factors. For example, a model $p_{\text{dis}}^{(1)}$ finetuned on more images might actually lose some non-semantic details compared to $p_{\text{dis}}^{(2)}$, which is finetuned on a single image. The extra p_{share} -based terms can thus be viewed as a correction that accounts for these mismatches in non-semantic content.

Following Zhang et al. (2024a)’s work, a good practical choice for p_{share} is often the pretrained model, because it has been trained on a large, diverse dataset and therefore captures broad, shared non-semantic features of images.

B.3 ESTIMATED DIFFERENCES OF KL DIVERGENCES

Because Δ depends on both the original concept \mathcal{C}_{ori} and the target class y_{tar} , enumerating every possible Δ would be impractical. Therefore, similar to the adversarial-example generation experiment introduced in Section 5.4, we restrict our analysis to the 30 target classes listed in Appendix E. We then compute the mean and variance of the estimated Δ (denoted $\tilde{\Delta}$), as shown in Table 4.

Table 4: Estimated differences of KL divergences $\tilde{\Delta}$ for each concept.

Concept name	$\tilde{\Delta}$	Concept name	$\tilde{\Delta}$	Concept name	$\tilde{\Delta}$
backpack	-3507.28 ± 2040.85	backpack_dog	-8372.57 ± 860.92	bear_plushie	-466.69 ± 1413.40
candle	-3637.39 ± 940.80	cat	-4658.98 ± 2423.05	cat2	-6654.28 ± 1318.03
colorful_sneaker	-4954.90 ± 420.40	dog	-7159.63 ± 696.25	dog2	-4814.63 ± 470.95
dog3	-8303.66 ± 2964.40	dog5	-8080.70 ± 2808.13	dog6	-2380.29 ± 1780.36
dog7	-10545.45 ± 787.79	dog8	-12401.76 ± 966.62	duck_toy	-2420.45 ± 2334.07
fancy_boot	-5780.99 ± 1489.92	grey_sloth_plushie	-6848.96 ± 1477.16	monster_toy	-7435.54 ± 1698.99
pink_sunglasses	-5711.26 ± 799.22	poop_emoji	-219.27 ± 929.88	rc_car	-5046.80 ± 3212.23
robot_toy	-7008.27 ± 710.45	shiny_sneaker	-3203.81 ± 4447.21	teapot	-7327.87 ± 486.00
vase	-8806.76 ± 2435.28	wolf_plushie	-325.80 ± 2811.99		

C SENSITIVITY STUDY FOR SAMPLE SELECTION

As described in Section 4.2, when generating adversarial examples we first sample M candidate adversarial images and then select the “best” one. To investigate the effect of different values of M , we perform a sensitivity study. In this study, $|\mathcal{C}_{\text{ori}}|$ is set to either 1 or 30, while M is set to 1, 5, or 10. Note that $|\mathcal{C}_{\text{ori}}| = 1$ corresponds to ProbAttack (Zhang et al., 2024b).

From Table 5, we observe that as M increases, the white-box attack success rate rises significantly. In the $|\mathcal{C}_{\text{ori}}| = 1$ case, the transferability also increases as M grows. However, in the $|\mathcal{C}_{\text{ori}}| = 30$ case, increasing M results in a decrease in transferability. This happens because we employ a conservative strategy (introduced in Section 4.2) to pick images that just barely fool the classifier while preserving the original concept. Evidence of this conservative strategy can be seen in Table 6: when $|\mathcal{C}_{\text{ori}}| = 30$, increasing M yields higher image quality and greater similarity to the original image. In contrast, when $|\mathcal{C}_{\text{ori}}| = 1$, the ranking criterion is more influential during the sample selection stage, so the conservative strategy does not take effect. Consequently, as M grows, the image quality tends to decrease.

Table 5: Targeted attack success rates (%) on ImageNet classifiers. In the white-box setting, success is counted when the target class is the top prediction. For transferability, we report top 100 success rates, as top 1 success was uniformly low across all methods.

	$ C_{\text{ori}} = 1$ $M = 1$	$ C_{\text{ori}} = 1$ $M = 5$	$ C_{\text{ori}} = 1$ $M = 10$	$ C_{\text{ori}} = 30$ $M = 1$	$ C_{\text{ori}} = 30$ $M = 5$	$ C_{\text{ori}} = 30$ $M = 10$
White-box	Top1					
Resnet 50	26.03	50.38	59.23	81.41	96.28	97.82
Transferability	Top100					
VGG19	16.41	17.82	18.97	30.00	23.21	20.90
ResNet 152	21.79	23.97	26.79	43.85	37.69	35.13
DenseNet 161	26.67	30.26	33.08	53.08	44.10	41.03
Inception V3	16.03	17.44	18.21	22.95	19.36	19.87
EfficientNet B7	16.15	16.54	17.44	25.90	21.54	20.38
Adversarial Defence	Top100					
Inception V3 Adv	18.97	17.82	20.00	25.26	20.64	20.51
EfficientNet B7 Adv	16.54	17.95	21.03	33.72	27.82	24.74
Ensemble IncRes V2	14.10	14.87	17.31	24.74	18.08	17.44

Table 6: Quantitative comparison of similarity to the original images and no reference image quality metrics for unrestricted adversarial examples.

	Clean	$ C_{\text{ori}} = 1$ $M = 1$	$ C_{\text{ori}} = 1$ $M = 5$	$ C_{\text{ori}} = 1$ $M = 10$	$ C_{\text{ori}} = 30$ $M = 1$	$ C_{\text{ori}} = 30$ $M = 5$	$ C_{\text{ori}} = 30$ $M = 10$
Similarity							
↑ User Study	N/A	N/A	N/A	0.8041	N/A	N/A	0.9654
↑ Avg. Clip Score	1.0	0.8953	0.8859	0.8581	0.8175	0.8286	0.8283
Image Quality							
↑ MUSIQ-KoniQ	65.0549	59.0779	59.7026	58.1563	62.8293	63.8795	63.7486
↑ MUSIQ-AVA	4.3760	4.3016	4.3400	4.3130	4.5013	4.5356	4.5305
↑ TReS	93.2127	86.4084	86.9480	84.3131	88.9667	90.6312	90.4488
↑ NIMA-AVA	4.5595	4.5729	4.5851	4.5168	4.6804	4.7422	4.7575
↑ HyperIQA	0.7255	0.6800	0.6808	0.6675	0.6880	0.6952	0.6947
↑ DBCNN	0.6956	0.6303	0.6340	0.6161	0.6459	0.6564	0.6572
↑ ARNIQA	0.7667	0.7222	0.7153	0.7009	0.7187	0.7323	0.7335

D FINETUNING DETAILS

In this section, we provide the key parameters required to fine-tune the models. For all parameters, please refer to the code repository of this paper.

D.1 FINETUNING DETAILS OF SDXL LORAS

In the SDXL LoRA finetuning described in Section 4.1 and Section 5.1, we use a LoRA rank of 128 with a corresponding LoRA alpha of 128, and set the dropout rate to 0.05. We employ the AdamW optimizer and train for 250 epochs, using a learning rate of 10^{-4} for UNet parameters and 10^{-5} for text encoder parameters. For more detailed settings, please refer to the accompanying code.

D.2 FINETUNING DETAILS OF DISTANCE DISTRIBUTIONS

For the diffusion model fine-tuning described in Section 5.2, we set the learning rate to 10^{-6} , use the AdamW optimizer, and train for 8000 steps per image in the fine-tuning set. More details are in the code repository.

E LIST OF THE SELECTED TARGET CLASSES

Since ImageNet consists of 1000 classes and it is impractical to cover them all, we randomly selected 30 target classes. For details, please refer to Table 7.

Table 7: List of the selected target classes

Index	Description
1	goldfish, <i>Carassius auratus</i>
2	great white shark, white shark, man-eater, man-eating shark, <i>Carcharodon carcharias</i>
7	cock
56	king snake, kingsnake
134	crane
151	Chihuahua
157	papillon
231	collie
254	basenji
309	bee
328	sea urchin
333	hamster
341	hog, pig, grunter, squealer, <i>Sus scrofa</i>
345	hippopotamus, hippo, river horse, <i>Hippopotamus amphibius</i>
368	gibbon, <i>Hylobates lar</i>
388	giant panda, panda, panda bear, coon bear, <i>Ailuropoda melanoleuca</i>
404	airliner
407	ambulance
417	balloon
504	coffee mug
555	fire engine, fire truck
563	fountain pen
620	laptop, laptop computer
721	pillow
769	rule, ruler
817	sports car, sport car
894	wardrobe, closet, press
947	mushroom
955	jackfruit, jak, jack
963	pizza, pizza pie

F DETAILS OF THE USER STUDY

We employed a crowdsourcing approach by hiring five annotators to determine whether each adversarial example preserves the original concept. Since our concepts are all concrete objects, we used the term “same item” to convey the notion of “same concept” in a straightforward manner. Following the user study methods of Song et al. (2018) and Zhang et al. (2024b), all five annotators voted on whether they believed each adversarial example still represented the original concept.

Annotator Instructions.

In this study, you will see two images and be asked whether they show the “same item.” Please follow these guidelines when making your judgment:

1. Shape/Form

- If the overall shape (including any accessories) in both images closely matches or approximates each other, answer “*Yes*.”
- If the object in one image appears excessively distorted or deformed compared to the other, answer “*No*.”

2. Accessories

- Even if the second image has additional or fewer accessories, as long as it essentially represents the same item, answer “*Yes*.”

3. Color

- If there is no significant difference in color between the two images, answer “*Yes*.”
- If there is a clear and noticeable color difference that affects recognizing the item, answer “*No*.”

Figure 4 shows the user interface for this study.

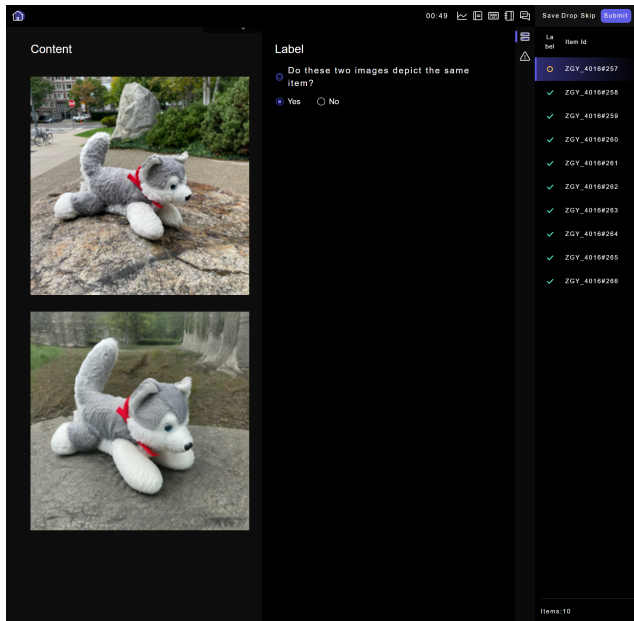


Figure 4: Screenshot of the user interface for user study.

G DETAILED QUALITATIVE ANALYSIS

Due to space constraints, the qualitative comparison figures in the main text are relatively small. Therefore, in this section, we present enlarged qualitative comparisons between DiffAttack and our approach. We focus on comparing DiffAttack in particular because, although it achieves a high target attack success rate, it produces lower-quality images, as shown in our user study and image quality tests. Here, we examine specific adversarial examples generated by DiffAttack to illustrate why its image quality is inferior.

- **Border Collie (first column of Figure 5).** DiffAttack removes all the dog’s fur details and replaces its eyes with those of another canine, while the nose and tongue become stylized with a graffiti-like look, losing realistic details. In contrast, although our concept-based adversarial example changes the dog’s pose, it preserves the animal’s fur and facial details.
- **Shiny Sneakers (second column).** DiffAttack turns the sneakers into a shoe design with sharp edges, losing the smooth curves of the original model.
- **Chow Chow (third column).** DiffAttack alters all of the fur details and erases the dog’s forelegs, resulting in a shape that resembles a drumstick rather than a chow chow.
- **Colorful Sneakers (fourth column).** While DiffAttack retains the purple front section and the blue rear section, it removes the yellow line in the middle and the adjacent cyan trim. Without these details, the sneaker’s appearance changes to a different style altogether.
- **Cat (fifth column).** DiffAttack modifies the cat’s fur patterns and gives it a distorted facial expression.

These observations further show that DiffAttack’s adversarial examples degrade crucial details, resulting in a significant drop in image quality and diminished fidelity to the original concept. **To emphasize that this qualitative study is not cherry-picking, we provide the complete set of adversarial examples — both from other methods and ours — in the code repository.**

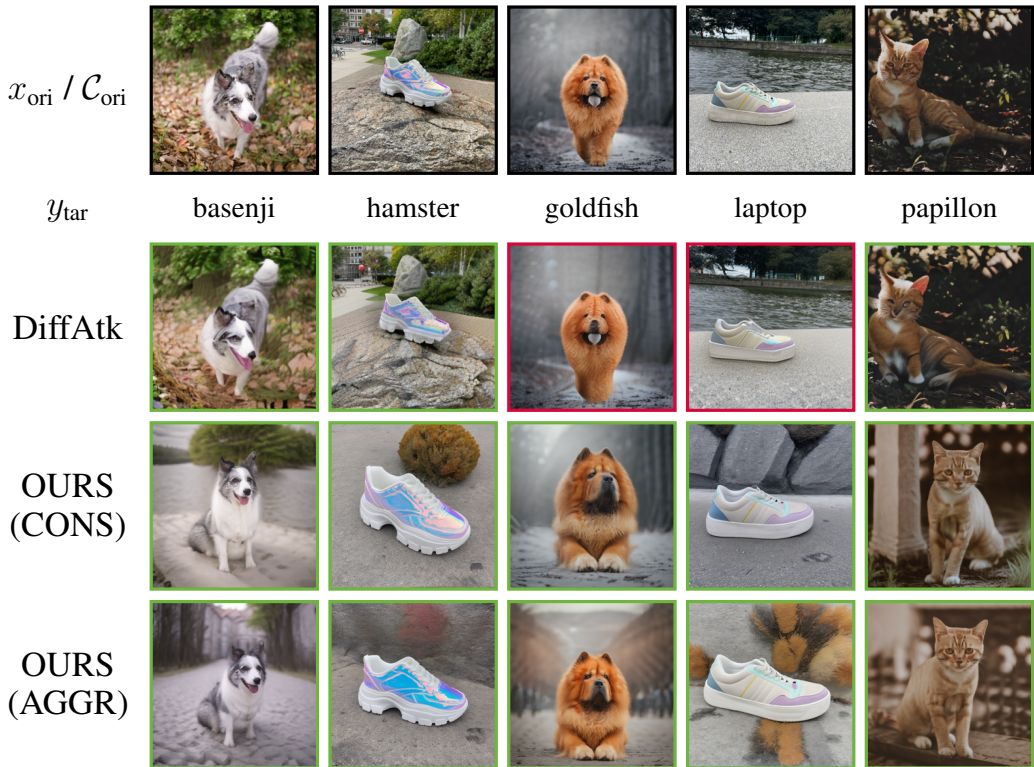


Figure 5: Qualitative comparison (zoomed in). (A **green** border indicates an example that successfully fools the classifier; **red** indicates failure.)

H ADDITIONAL COMMENTS ON TRANSFERABILITY

As shown in Appendix Q, our proposed method consistently achieves the best transferability among comparable approaches. However, its attack success rates are still considerably lower than those of methods explicitly optimized for transferability, such as works of Zhu et al. (2022), Wang & He (2021), Gubri et al. (2022) and Collins et al. (2025). We note that approaches targeting transferability often generate clear visual features of the target class. Especially in the setting of unrestricted adversarial attacks, directly synthesizing objects of the target class within the image is also considered valid (see Figure 5 in the appendix of Collins et al. (2025)).

From the probabilistic perspective of adversarial attack, this phenomenon is especially intuitive. As illustrated in Figure 6, p_{dis} denotes the distance distribution, while $p_{\text{vic}}^{(1)}$ and $p_{\text{vic}}^{(2)}$ represent the victim distributions induced by two different classifiers. Without loss of generality, suppose adversarial examples are sampled from the product of the red distribution $p_{\text{vic}}^{(1)}$ and the blue distribution p_{dis} . The resulting adversarial examples concentrate in the region where these two distributions overlap. As shown in the figure, this region corresponds to low probability density under the green distribution $p_{\text{vic}}^{(2)}$, leading to poor transferability across classifiers.

Although the overall transferability of our method is relatively low, expanding p_{dis} indeed brings the overlap between the blue and red distributions closer to the green distribution, making it reasonable that a larger p_{dis} leads to an improvement in transferability.

However, it is important to emphasize that our goal fundamentally differs from methods explicitly designed to maximize transferability. Approaches that achieve very high transferability, such as Zhu et al. (2022) and Collins et al. (2025), typically introduce strong visual features of the target class. Doing so moves samples toward the intersection of the red and green victim distributions, thereby dramatically improving transferability. Yet this strategy comes at the cost of injecting target-

class semantics into the generated images, which directly violates our requirement of preserving the original identity-level concept.

In contrast, our method aims to investigate how enlarging the concept-based distance distribution p_{dis} affects both image quality and transferability, while strictly maintaining the underlying identity. Under this constraint, extremely high transferability is not expected - and, in fact, cannot be achieved without compromising identity preservation. Although our framework could be extended to incorporate target-class features to boost transferability, we view this as beyond the scope of the current work and a promising direction for future research.

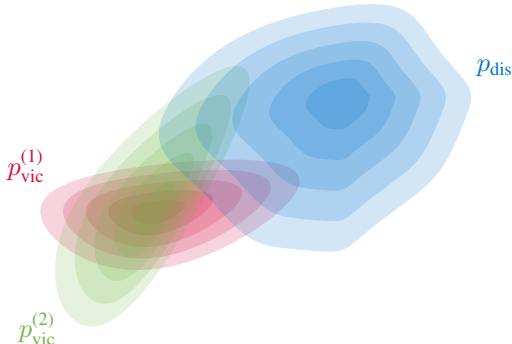


Figure 6: Transferability of adversarial attacks from a probabilistic perspective. p_{dis} denotes the distance distribution, while $p_{\text{vic}}^{(1)}$ and $p_{\text{vic}}^{(2)}$ represent the victim distributions induced by two different classifiers. Without loss of generality, assume that adversarial examples are sampled from the product of the red distribution $p_{\text{vic}}^{(1)}$ and the blue distribution p_{dis} . In this case, the generated adversarial examples concentrate in the overlap between these two distributions. As illustrated in the figure, this overlapping region has low probability density under the green distribution $p_{\text{vic}}^{(2)}$, resulting in poor transferability. Moreover, if a sample happens to contain strong visual evidence of the target class, then both classifiers would classify it as the target with high confidence, hence the high-density regions of $p_{\text{vic}}^{(1)}$ and $p_{\text{vic}}^{(2)}$ would necessarily overlap.

I COMPUTE RESOURCES

All experiments are conducted on a single NVIDIA H100 Tensor Core GPU. Our method requires approximately 20 minute per concept for concept augmentation and around 8 hours per concept for diffusion model fine-tuning. For adversarial example generation, although our method is slightly slower, it is still within the same order of magnitude.

To ensure that the diffusion model learns a high-quality identity-level concept, we train it for a long duration during the concept finetuning stage. When the concept dataset is sufficiently large (e.g., the 30 images described in the main text), the diffusion model does not collapse even after many epochs of finetuning. However, in settings like ProbAttack, where finetuning is performed on a single image, the number of epochs must be carefully controlled to avoid model collapse. For this reason, the concept finetuning time for ProbAttack is approximately 20 minutes, whereas our concept-based method requires about 8 hours.

In our experiments, we ensured that this 8-hour finetuning worked reliably across all concepts studied in the paper. In practice, the finetuning time can be reduced to some extent; however, maintaining an identity-level concept is inherently subjective and difficult to quantify, making it challenging to specify a universally optimal finetuning duration.

Table 8 summarizes the time consumption of different methods across concept augmentation, concept fine-tuning, and adversarial example generation stages.

Table 8: Time consumption of each method across different stages.

	NCF	ACA	DiffAttack	ProbAttack	OURS
Concept augmentation (per concept)	-	-	-	-	20m
Concept finetune (per concept)	-	-	-	20m	8h
Adversarial example generation (per image)	30s	20s	12s	75s	75s

J DATASETS AND LICENSES

In this work, we use the DreamBooth dataset, which is licensed under the Creative Commons Attribution 4.0 International license.

K PRACTICAL USAGE GUIDELINES AND EXAMPLE SCENARIOS

K.1 GUIDELINES

Although the term “concept” is difficult to define precisely, our method provides a clear definition: a concept can be specified by either a set \mathcal{C}_{ori} or a probabilistic model. Users can therefore construct \mathcal{C}_{ori} to include whatever concept variations they desire. In our experiments, we demonstrate a broad range of concept variations — background, pose, and viewpoint — leading to a highly diverse \mathcal{C}_{ori} and scenarios like the one shown in Figure 1 (right).

In practice, constraints may prevent such extensive concept variations. For example, one might need to fix the background and viewpoint, leaving only the object’s pose or special variations (e.g., dressing a dog in different outfits). However, if the concept variations are too limited, the intersection between p_{dis} and p_{vic} may be insufficient, making it harder to generate adversarial samples. Practitioners should be mindful of this trade-off.

K.2 EXAMPLE SCENARIOS

K.2.1 SCENARIO 1: PROHIBITED ITEM ADVERTISEMENTS ON SOCIAL PLATFORMS

Social or second-hand platforms often employ basic classifiers to preliminarily filter user-uploaded content for prohibited items (e.g., firearms, knives, protected animals). Malicious actors aim to sell prohibited items such as a specific brand and model of firearm, a particular knife, or a specific protected animal cub. They prefer to upload images capturing all detailed features of the prohibited items (i.e., preserving concept/identity, such as the specific firearm model or exact animal cub) to attract precise target buyers while bypassing platform moderation (untargeted attack).

In such cases, preserving the concept and identity is crucial to attracting potential customers, while background and perspective variations in images are insignificant. This perfectly aligns with the applicability of concept-based adversarial attacks.

Considering the potential societal harm of this scenario, as previously discussed, social platforms should implement multiple detection systems, including AI-based detection, to prevent such attacks.

K.2.2 SCENARIO 2: IMPERCEPTIBLE ADVERSARIAL PATCHES IN REAL-WORLD SCENARIOS (ADVERSARIAL PATCH T-SHIRTS)

In practice, adversarial examples may be printed as patches. Early adversarial patches, though able to evade classifiers or detectors, often appeared unnatural or suspicious, making them easily noticeable by humans and limiting their effectiveness. Creating imperceptible adversarial patches remains a significant challenge.

Our method addresses this challenge by adopting brand images, logos, or cartoon characters as the concept. By altering the background or viewpoint of these concepts, we create realistic adversarial patches suitable for real-world applications.

More concretely, as demonstrated by Wang et al. (2024), adversarial examples can be created as printed patches on T-shirts to deceive detection systems. However, unnatural or suspicious patches would prompt humans to comment, “You’re wearing a strange T-shirt,” or, “The logo on your T-shirt looks odd.” In such scenarios, our concept-based adversarial attack excels by preserving logos, branding, or cartoon imagery while subtly changing the background or making the characters perform specific actions, resulting in adversarial patches that are difficult for humans to detect.

Specifically referencing Wang et al. (2024)’s work, their algorithm primarily focuses on single-image adversarial patch creation, leading to unnatural-looking printed watermarks on T-shirts. In contrast, our concept-based adversarial attack provides a better solution.

Given the social harm posed by these attacks, real-world detection systems should employ multi-layered detection with varying thresholds and multiple scales of analysis to prevent such vulnerabilities.

L NEGATIVE SOCIAL EFFECT AND MITIGATION STRATEGIES

Mitigating the risks of our proposed attack is a crucial responsibility for both the machine learning community and society. Potential strategies include:

- Adversarial training using concept-based adversarial examples is a direct and general mitigation strategy. However, this may come at the cost of reduced baseline model accuracy.
- Given that our adversarial examples are directly generated from probabilistic generative models, contemporary AI-generated content detection techniques (open-source/commercial), such as frequency-domain analysis, heatmap analysis, anomaly detection, and counterfactual detection, can serve as effective countermeasures.
- In practical engineering scenarios, combining various methods according to specific application needs can significantly mitigate the threat posed by this attack.

The field of adversarial attacks continually evolves through the ongoing advancement of both attack and defense strategies. We hope our novel attack method draws sufficient attention from the community to further enhance AI Safety research.

M BROADER IMPACTS OF THIS WORK

This study introduces concept-based adversarial attacks, providing valuable insights into the vulnerabilities of sophisticated classifiers.

On the positive side, our work exposes critical weaknesses in systems previously considered robust, highlighting the need for enhanced security measures in classifier design. By identifying these vulnerabilities, we contribute to the development of more resilient artificial intelligence systems.

However, we acknowledge potential negative implications. The concept-based attack methods described could be misappropriated by malicious actors, for example, for identification purposes. We emphasize the importance of developing countermeasures against such exploitation and encourage the research community to consider ethical implications when building upon this work.

N LLM DISCLAIMER

In this work, we use large language models solely for text polishing.

O LIMITATIONS

Our approach is slower than similar methods because it requires time-consuming fine-tuning on a concept dataset \mathcal{C}_{ori} , which may also need to be built or expanded if unavailable. However, in adversarial attack scenarios, even one successful example can cause severe damage, highlighting the practical importance of our method.

Method	Sampler / Solver	# Sampling Steps	# Attack Steps	Step Size	Notes
DiffAttack	DDIM	50	30	0.01	–
ACA	DDIM	50	10	0.04	–
NCF	–	–	15	0.013	# Color Sampling = 10
ProbAttack	DDPM	250	–	–	$ C_{\text{ori}} = 1, M = 10, c = 30.$
Concept-based	DDPM	250	–	–	$ C_{\text{ori}} = 30, M = 10, c = 30.$

Table 9: Hyperparameter settings for all compared methods. ProbAttack and our concept-based adversarial attack both use the standard stochastic diffusion (DDPM) sampler with classifier-guided Langevin dynamics, not DDIM. All other parameters are at default.

P BASELINE SETTINGS

We list the hyperparameter settings for all compared methods in Table 9. Note that DiffAttack/ACA and ProbAttack/Concept-based Attack rely on fundamentally different attack mechanisms: the former are based on DDIM and operate in the latent space, while the latter directly sample from p_{adv} . As a result, the number of sampling steps is not directly comparable across these methods, and the latter do not require any additional attack steps.

Q FULL MAIN EXPERIMENTAL RESULTS

Due to space constraints, the main text reports only the white-box Top-1 and black-box Top-5 results using ResNet-50 as the surrogate classifier. In this section, we provide the full set of experimental results, including targeted attack success rates (white-box Top-1, black-box Top-1, Top-5, Top-10, and Top-100) in Section Q.1, and the similarity and image quality evaluations in Section Q.2.

Q.1 TARGETED ATTACK SUCCESS RATES

Table 10: Attack success rates (%) on ImageNet classifiers, with ResNet-50 serving as the white-box victim (surrogate) classifier.

	NCF	ACA	DiffAttack	ProbAttack	OURS (CONS)	OURS (AGGR)
White-box						
Targeted-Top1						
ResNet 50	1.15	6.03	84.23	59.23	97.82	97.82
Transferability						
VGG19	0.26	0.26	1.67	0.38	0.00	1.15
ResNet 152	0.13	0.38	1.79	0.77	0.26	1.79
DenseNet 161	0.00	0.26	1.67	0.51	0.26	2.82
Inception V3	0.13	0.13	0.90	0.51	0.00	1.54
EfficientNet B7	0.00	0.26	0.38	0.00	0.13	1.15
Adversarial Defence						
ResNet 50 Adv	0.00	0.38	0.77	0.26	0.00	1.15
Inception V3 Adv	0.00	0.26	1.03	0.26	0.00	1.03
EfficientNet B7 Adv	0.00	0.51	0.64	0.38	0.26	1.41
Ensemble IncRes V2	0.00	0.26	0.38	0.64	0.00	1.28
White-box						
Targeted-Top5						
ResNet 50	3.21	10.64	90.64	72.82	99.87	99.87
Transferability						
VGG19	1.28	1.67	4.36	2.44	2.05	4.36
ResNet 152	1.41	1.92	8.33	3.33	2.82	8.72
DenseNet 161	1.41	2.05	7.44	3.97	3.85	11.54
Inception V3	0.90	1.41	3.08	2.56	1.28	4.74
EfficientNet B7	1.41	1.67	1.79	1.41	1.28	3.97
Adversarial Defence						
ResNet 50 Adv	0.90	1.15	3.46	2.56	1.79	5.64
Inception V3 Adv	1.15	1.28	3.21	2.18	0.90	3.72
EfficientNet B7 Adv	0.26	1.15	2.05	2.31	1.67	6.41
Ensemble IncRes V2	0.77	1.28	2.69	1.92	0.77	5.00
White-box						
Targeted-Top10						
ResNet 50	4.23	12.69	93.46	75.64	99.87	99.87
Transferability						
VGG19	2.69	2.69	8.21	3.46	3.21	6.79
ResNet 152	2.44	3.59	14.74	5.77	6.28	15.13
DenseNet 161	2.31	3.72	12.69	6.15	8.72	19.62
Inception V3	1.28	2.31	5.13	3.46	2.31	6.54
EfficientNet B7	2.31	2.82	4.23	3.21	3.59	6.54
Adversarial Defence						
ResNet 50 Adv	1.41	1.92	5.64	3.59	2.69	8.46
Inception V3 Adv	1.79	1.79	5.13	3.46	2.31	6.54
EfficientNet B7 Adv	0.38	2.05	3.08	3.46	2.44	9.36
Ensemble IncRes V2	1.28	2.05	3.85	3.08	1.79	7.18

Table 11: Attack success rates (%) on ImageNet classifiers, with MobileNet v2 serving as the white-box victim (surrogate) classifier.

	NCF	ACA	DiffAttack	ProbAttack	OURS (CONS)	OURS (AGGR)
White-box	Targeted-Top1					
MN-V2	3.85	12.95	91.92	51.15	97.31	97.31
Transferability						
VGG19	0.00	0.13	1.79	0.00	0.00	1.54
ResNet 152	0.13	0.26	0.90	0.13	0.00	1.03
DenseNet 161	0.00	0.26	0.90	1.03	0.00	1.28
Inception V3	0.00	0.13	0.51	0.38	0.00	0.90
EfficientNet B7	0.00	0.00	0.64	0.13	0.13	1.28
Adversarial Defence						
Inception V3 Adv	0.00	0.26	0.77	0.13	0.13	1.15
EfficientNet B7 Adv	0.00	0.26	0.26	0.26	0.38	1.41
Ensemble IncRes V2	0.00	0.38	0.77	0.26	0.13	1.28
White-box	Targeted-Top5					
MN-V2	6.41	17.18	95.64	65.64	99.74	99.74
Transferability						
VGG19	1.03	2.05	4.36	1.54	1.92	4.74
ResNet 152	1.15	1.54	3.72	1.79	1.92	4.87
DenseNet 161	1.15	1.54	5.51	3.46	2.56	7.18
Inception V3	0.90	1.15	2.44	1.92	1.79	3.97
EfficientNet B7	1.03	1.41	2.05	0.51	0.90	4.36
Adversarial Defence						
Inception V3 Adv	0.90	1.15	2.56	1.67	0.90	3.08
EfficientNet B7 Adv	0.38	1.15	1.92	1.54	1.41	5.77
Ensemble IncRes V2	0.38	1.67	2.56	1.15	0.90	4.36
White-box	Targeted-Top10					
MN-V2	8.33	20.00	97.05	72.31	99.74	99.74
Transferability						
VGG19	1.28	2.95	7.31	2.69	3.33	6.92
ResNet 152	1.54	2.56	7.05	3.59	2.82	8.08
DenseNet 161	1.67	3.08	9.10	5.00	4.36	12.44
Inception V3	1.41	2.82	4.23	2.82	2.82	5.90
EfficientNet B7	1.79	3.33	3.72	2.18	3.08	7.31
Adversarial Defence						
Inception V3 Adv	1.28	1.41	4.10	2.56	2.05	5.90
EfficientNet B7 Adv	0.64	2.44	3.59	2.82	3.97	8.72
Ensemble IncRes V2	0.77	2.31	3.72	2.95	2.31	7.18

Table 12: Attack success rates (%) on ImageNet classifiers, with ViT-Base serving as the white-box victim (surrogate) classifier.

	NCF	ACA	DiffAttack	ProbAttack	OURS (CONS)	OURS (AGGR)
White-box	Targeted-Top1					
ViT-B	0.90	3.46	81.41	63.85	85.51	85.51
Transferability						
VGG19	0.13	0.26	0.51	0.13	0.13	1.28
ResNet 152	0.00	0.38	0.77	0.00	0.00	1.41
DenseNet 161	0.00	0.26	1.15	0.51	0.00	1.15
Inception V3	0.00	0.38	0.38	0.13	0.13	0.64
EfficientNet B7	0.00	0.26	0.64	0.00	0.00	0.77
Adversarial Defence						
Inception V3 Adv	0.00	0.26	0.38	0.13	0.13	0.90
EfficientNet B7 Adv	0.00	0.38	0.90	0.51	0.51	1.15
Ensemble IncRes V2	0.00	0.13	1.03	0.13	0.00	1.15
White-box	Targeted-Top5					
ViT-B	2.44	6.67	92.44	89.74	94.87	94.87
Transferability						
VGG19	1.03	1.41	1.79	1.28	1.41	3.33
ResNet 152	0.64	1.67	3.33	1.03	1.67	4.74
DenseNet 161	0.64	1.67	4.87	2.18	1.67	5.51
Inception V3	0.77	1.41	2.95	1.54	0.90	3.08
EfficientNet B7	0.90	1.92	2.69	1.28	1.15	3.08
Adversarial Defence						
Inception V3 Adv	0.51	1.92	3.21	0.64	0.90	3.46
EfficientNet B7 Adv	0.26	1.79	3.08	1.67	1.41	3.85
Ensemble IncRes V2	0.51	1.41	3.08	1.28	0.90	3.21
White-box	Targeted-Top10					
ViT-B	3.46	8.97	95.13	92.05	95.51	95.51
Transferability						
VGG19	1.79	2.69	3.46	2.05	2.82	4.49
ResNet 152	1.28	1.92	5.77	2.05	2.82	7.69
DenseNet 161	1.15	2.82	6.92	3.08	4.23	8.59
Inception V3	1.28	2.05	4.87	1.79	1.92	5.00
EfficientNet B7	1.54	2.95	4.49	2.44	3.21	5.64
Adversarial Defence						
Inception V3 Adv	0.77	2.18	5.13	2.44	2.05	5.26
EfficientNet B7 Adv	0.38	2.31	5.51	2.82	3.33	6.03
Ensemble IncRes V2	0.90	2.31	4.87	2.31	2.56	5.00

Table 13: Attack success rates (%) on ImageNet classifiers, with ConvNext serving as the white-box victim (surrogate) classifier.

	NCF	ACA	DiffAttack	ProbAttack	OURS (CONS)	OURS (AGGR)
White-box						
Targeted-Top1						
ConvNext	1.03	5.38	83.59	60.38	94.74	94.74
Transferability						
VGG19	0.00	0.26	1.28	0.26	0.00	1.15
ResNet 152	0.00	0.38	1.54	0.51	0.13	1.67
DenseNet 161	0.00	0.26	1.54	0.51	0.13	2.31
Inception V3	0.13	0.26	0.77	0.38	0.00	1.28
EfficientNet B7	0.00	0.26	0.51	0.00	0.13	1.03
Adversarial Defence						
Inception V3 Adv	0.00	0.26	0.90	0.26	0.00	1.03
EfficientNet B7 Adv	0.00	0.51	0.77	0.38	0.38	1.28
Ensemble IncRes V2	0.00	0.26	0.51	0.51	0.00	1.28
White-box						
Targeted-Top5						
ConvNext	2.95	9.36	91.15	78.85	98.59	98.59
Transferability-Top5						
VGG19	1.15	1.54	3.46	2.05	1.79	4.10
ResNet 152	1.15	1.79	6.92	2.69	2.44	7.56
DenseNet 161	1.15	1.92	6.67	3.33	3.21	9.62
Inception V3	0.90	1.41	3.08	2.18	1.15	4.23
EfficientNet B7	1.28	1.79	2.05	1.41	1.28	3.72
Adversarial Defence						
Inception V3 Adv	0.90	1.41	3.21	1.67	0.90	3.59
EfficientNet B7 Adv	0.26	1.28	2.44	2.05	1.54	5.51
Ensemble IncRes V2	0.64	1.28	2.82	1.67	0.77	4.49
White-box						
Targeted-Top10						
ConvNext	3.97	11.67	93.97	81.54	98.72	98.72
Transferability						
VGG19	2.44	2.69	6.67	2.95	3.08	6.15
ResNet 152	2.05	3.08	11.92	4.49	5.13	12.82
DenseNet 161	1.92	3.46	10.90	5.13	7.18	16.41
Inception V3	1.28	2.18	5.00	2.82	2.18	6.15
EfficientNet B7	2.05	2.82	4.36	2.95	3.46	6.28
Adversarial Defence						
Inception V3 Adv	1.41	1.92	5.13	3.08	2.18	6.15
EfficientNet B7 Adv	0.38	2.18	3.72	3.21	2.69	8.21
Ensemble IncRes V2	1.15	2.18	4.23	2.82	2.05	6.54

Table 14: Attack success rates (%) on ImageNet classifiers, with ResNet-50 Adv serving as the white-box victim (surrogate) classifier.

	NCF	ACA	DiffAttack	ProbAttack	OURS (CONS)	OURS (AGGR)
White-box	Targeted-Top1					
ResNet-50 Adv	0.90	5.13	81.79	61.28	94.23	94.23
Transferability						
VGG19	0.13	0.38	1.67	0.51	0.00	2.31
ResNet 152	0.00	0.51	2.56	1.03	0.38	2.56
DenseNet 161	0.00	0.38	2.31	0.77	0.38	3.97
Inception V3	0.00	0.26	1.28	0.77	0.00	2.18
EfficientNet B7	0.00	0.38	0.51	0.00	0.26	1.67
Adversarial Defence						
Inception V3 Adv	0.00	0.51	1.67	0.51	0.00	1.79
EfficientNet B7 Adv	0.00	0.90	1.15	0.64	0.51	2.56
Ensemble IncRes V2	0.00	0.51	0.64	1.15	0.00	2.31
White-box	Targeted-Top5					
ResNet-50 Adv	2.82	9.62	89.74	75.00	98.08	98.08
Transferability						
VGG19	1.03	2.31	5.77	3.33	2.82	6.15
ResNet 152	1.15	2.69	11.28	4.49	3.85	11.79
DenseNet 161	1.15	2.82	10.00	5.38	5.26	15.38
Inception V3	0.77	1.92	4.36	3.46	1.79	6.67
EfficientNet B7	1.15	2.31	2.56	1.92	1.79	5.51
Adversarial Defence						
Inception V3 Adv	0.90	1.92	5.13	3.46	1.41	6.15
EfficientNet B7 Adv	0.26	1.79	3.33	3.59	2.56	10.00
Ensemble IncRes V2	0.64	1.92	4.36	3.08	1.15	7.95
White-box	Targeted-Top10					
ResNet-50 Adv	3.85	11.67	92.95	77.56	98.97	98.97
Transferability						
VGG19	2.18	3.72	8.97	4.62	4.36	10.77
ResNet 152	2.05	4.87	18.97	7.44	8.08	19.49
DenseNet 161	1.92	5.00	16.28	7.95	11.15	25.13
Inception V3	1.03	3.21	6.92	4.62	3.08	8.72
EfficientNet B7	1.92	3.85	5.64	4.36	4.87	8.72
Adversarial Defence						
Inception V3 Adv	1.41	2.69	8.21	5.38	3.59	10.51
EfficientNet B7 Adv	0.38	3.08	5.00	5.38	3.85	14.74
Ensemble IncRes V2	1.03	3.08	6.15	4.74	2.82	11.41

Q.2 SIMILARITY AND IMAGE QUALITY

Due to cost constraints, only the ResNet-50 results reported in the main text include the user study.

Table 15: Quantitative comparison of similarity to the original images and no reference image quality metrics for unrestricted adversarial examples with ResNet-50 serving as the victim (surrogate) classifier.

	Clean	NCF	ACA	DiffAttack	ProbAttack	OURS (CONS)	OURS (AGGR)
Similarity							
↑ User Study	N/A	0.1859	0.2808	0.7577	0.8041	0.9654	0.8808
↑ Avg. Clip Score	1.0	0.8728	0.7861	0.8093	0.8581	0.8283	0.8043
Image Quality							
↑ HyperIQA	0.7255	0.5075	0.6462	0.5551	0.6675	0.6947	0.6809
↑ DBCNN	0.6956	0.5096	0.6103	0.5294	0.6161	0.6572	0.6399
↑ ARNIQA	0.7667	0.5978	0.6879	0.6909	0.7009	0.7335	0.7154
↑ MUSIQ-AVA	4.3760	3.8135	4.2687	4.0734	4.3130	4.5305	4.5250
↑ NIMA-AVA	4.5595	3.7916	4.4511	4.0589	4.5168	4.7575	4.7401
↑ MUSIQ-KonIQ	65.0549	50.5022	59.0840	52.5399	58.1563	63.7486	62.2217
↑ TReS	93.2127	64.7050	85.8435	74.1167	84.3131	90.4488	88.0836

Table 16: Quantitative comparison of similarity to the original images and no reference image quality metrics for unrestricted adversarial examples with MN-V2 serving as the victim (surrogate) classifier.

	Clean	NCF	ACA	DiffAttack	ProbAttack	OURS (CONS)	OURS (AGGR)
Similarity							
↑ Avg. Clip Score	1.0	0.8783	0.7756	0.8197	0.8693	0.8229	0.7988
Image Quality							
↑ HyperIQA	0.7255	0.5002	0.6486	0.5471	0.6808	0.6998	0.6865
↑ DBCNN	0.6956	0.5040	0.6175	0.5236	0.6310	0.6577	0.6402
↑ ARNIQA	0.7667	0.5972	0.6909	0.6872	0.7112	0.7328	0.7142
↑ MUSIQ-AVA	4.3760	3.7912	4.3042	4.0496	4.3236	4.6125	4.5700
↑ NIMA-AVA	4.5595	3.7879	4.4532	4.0549	4.5317	4.8172	4.7778
↑ MUSIQ-KonIQ	65.0549	49.9072	59.5258	51.9209	59.7813	63.5363	61.6641
↑ TReS	93.2127	63.7643	86.2644	73.0392	86.4376	90.7757	88.9947

Table 17: Quantitative comparison of similarity to the original images and no reference image quality metrics for unrestricted adversarial examples with ViT-Base serving as the victim (surrogate) classifier.

	Clean	NCF	ACA	DiffAttack	ProbAttack	OURS (CONS)	OURS (AGGR)
Similarity							
↑ Avg. Clip Score	1.0	0.8733	0.7681	0.8040	0.8586	0.8222	0.8104
Image Quality							
↑ HyperIQA	0.7255	0.5006	0.6324	0.5475	0.6796	0.7077	0.6961
↑ DBCNN	0.6956	0.5027	0.5842	0.5222	0.6254	0.6652	0.6526
↑ ARNIQA	0.7667	0.5879	0.6765	0.6844	0.7120	0.7351	0.7195
↑ MUSIQ-AVA	4.3760	3.7822	4.3131	4.0400	4.2450	4.5401	4.5345
↑ NIMA-AVA	4.5595	3.7666	4.4775	4.0321	4.4918	4.7706	4.7747
↑ MUSIQ-KonIQ	65.0549	50.0413	57.6105	52.0604	59.3605	64.2536	62.4264
↑ TReS	93.2127	64.1109	83.6834	73.4362	85.8749	91.7463	89.7815

Table 18: Quantitative comparison of similarity to the original images and no reference image quality metrics for unrestricted adversarial examples with ConvNeXT serving as the victim (surrogate) classifier.

	Clean	NCF	ACA	DiffAttack	ProbAttack	OURS (CONS)	OURS (AGGR)
Similarity							
↑ Avg. Clip Score	1.0	0.8621	0.7542	0.7964	0.8467	0.8139	0.8011
Image Quality							
↑ HyperIQ	0.7255	0.4928	0.6281	0.5392	0.6703	0.6933	0.6810
↑ DBCNN	0.6956	0.4951	0.5784	0.5179	0.6201	0.6531	0.6405
↑ ARNIQA	0.7667	0.5835	0.6710	0.6801	0.7066	0.7294	0.7118
↑ MUSIQ-AVA	4.3760	3.7511	4.2814	4.0206	4.2314	4.5116	4.5030
↑ NIMA-AVA	4.5595	3.7524	4.4433	4.0215	4.4830	4.7464	4.7492
↑ MUSIQ-KonIQ	65.0549	49.3812	57.0114	51.7324	58.9012	63.1025	61.3571
↑ TReS	93.2127	62.9011	82.7410	72.1109	85.2442	90.9211	88.7724

Table 19: Quantitative comparison of similarity to the original images and no reference image quality metrics for unrestricted adversarial examples with ResNet-50 Adv. serving as the victim (surrogate) classifier.

	Clean	NCF	ACA	DiffAttack	ProbAttack	OURS (CONS)	OURS (AGGR)
Similarity							
↑ Avg. Clip Score	1.0	0.8556	0.7485	0.7877	0.8367	0.8059	0.7945
Image Quality							
↑ HyperIQ	0.7255	0.4854	0.6221	0.5297	0.6617	0.6875	0.6750
↑ DBCNN	0.6956	0.4908	0.5718	0.5070	0.6078	0.6473	0.6342
↑ ARNIQA	0.7667	0.5764	0.6654	0.6683	0.6932	0.7231	0.7070
↑ MUSIQ-AVA	4.3760	3.7435	4.2637	4.0130	4.2223	4.5031	4.4966
↑ NIMA-AVA	4.5595	3.7453	4.4342	4.0113	4.4676	4.7399	4.7351
↑ MUSIQ-KonIQ	65.0549	49.3740	57.0028	51.7202	58.1513	63.0946	61.3527
↑ TReS	93.2127	62.8961	82.7340	72.1034	84.3081	90.4438	88.0786